frontiers | Frontiers in Medicine

TYPE Review
PUBLISHED 05 October 2022
DOI 10.3389/fmed.2022.945602

OPEN ACCESS

EDITED BY
Takuya Toyonaga,
Yale University, United States

REVIEWED BY
Carmelo Caldarella,
Fondazione Policlinico Universitario A. Gemelli IRCCS, Italy
Markus Krönke,
Technical University Munich, Germany

*CORRESPONDENCE
Hong Fan
fanhongfan@qq.com
Xiaoai Wu
Xiaoai.wu@scu.edu.cn

†These authors have contributed equally to this work

SPECIALTY SECTION
This article was submitted to Nuclear Medicine, a section of the journal Frontiers in Medicine

RECEIVED 16 May 2022
ACCEPTED 31 August 2022
PUBLISHED 05 October 2022

CITATION
Zhu J, Pan F, Cai H, Pan L, Li Y, Li L, Li Y, Wu X and Fan H (2022) Positron emission tomography imaging of lung cancer: An overview of alternative positron emission tomography tracers beyond F18 fluorodeoxyglucose. *Front. Med.* 9:945602. doi: 10.3389/fmed.2022.945602

Positron emission tomography imaging of lung cancer: An overview of alternative positron emission tomography tracers beyond F18 fluorodeoxyglucose

Jing Zhu[1,2,3†], Fei Pan[4†], Huawei Cai[4], Lili Pan[4], Yalun Li[1], Lin Li[4], YunChun Li[4,5], Xiaoai Wu[4*] and Hong Fan[1*]

[1]Department of Respiratory and Critical Care Medicine, West China Hospital, Sichuan University, Chengdu, China, [2]Respiratory and Critical Care Medicine, Mianyang Central Hospital, School of Medicine, University of Electronic Science and Technology of China, Mianyang, China, [3]NHC Key Laboratory of Nuclear Technology Medical Transformation, Mianyang Central Hospital, School of Medicine, University of Electronic Science and Technology of China, Mianyang, China, [4]Department of Nuclear Medicine, Laboratory of Clinical Nuclear Medicine, West China Hospital, Sichuan University, Chengdu, China, [5]Department of Nuclear Medicine, The Second People's Hospital of Yibin, Yibin, China

Lung cancer has been the leading cause of cancer-related mortality in China in recent decades. Positron emission tomography-computer tomography (PET/CT) has been established in the diagnosis of lung cancer. ^{18}F-FDG is the most widely used PET tracer in foci diagnosis, tumor staging, treatment planning, and prognosis assessment by monitoring abnormally exuberant glucose metabolism in tumors. However, with the increasing knowledge on tumor heterogeneity and biological characteristics in lung cancer, a variety of novel radiotracers beyond ^{18}F-FDG for PET imaging have been developed. For example, PET tracers that target cellular proliferation, amino acid metabolism and transportation, tumor hypoxia, angiogenesis, pulmonary NETs and other targets, such as tyrosine kinases and cancer-associated fibroblasts, have been reported, evaluated in animal models or under clinical investigations in recent years and play increasing roles in lung cancer diagnosis. Thus, we perform a comprehensive literature review of the radiopharmaceuticals and recent progress in PET tracers for the study of lung cancer biological characteristics beyond glucose metabolism.

KEYWORDS

PET, lung cancer, ^{18}F-FDG, radiotracer, tyrosine kinases inhibitor

Introduction

Lung cancer (LC) is a major threat to public health, accounting for the highest cancer-related mortality among all types of cancers worldwide (1, 2). Based on histological differences, LC can mainly be classified into small-cell lung carcinoma (SCLC), non-small-cell lung cancer (NSCLC) and pulmonary neuroendocrine tumors (NETs) (3, 4). NSCLC accounts for approximately 85–90% of all LC incidences and includes squamous-cell carcinoma (SCC), adenocarcinoma, and large-cell carcinoma (5). In the last century, the overall 5-year survival rates for LC patients remain relatively low, since LC is often advanced to the late stage when diagnosed and the treatments are limited under those circumstances (2, 6). Fortunately, inspiring improvements in survival rates of LC have been achieved in recent decades, which benefited from the development of molecular imaging technologies, including positron emission tomography (PET) (7, 8).

Compared with conventional X-ray and CT, PET has the advantages of tumor targeting and effective quantitative capabilities and thus is more powerful in detecting functional abnormalities in lung cancer diagnosis (9–11).

As an analog of glucose, ^{18}F-fluorodeoxyglucose (^{18}F-FDG) is the most commonly used PET tracer for the detection of solid tumors. ^{18}F-FDG accumulates in tumor cells *via* membrane glucose transporters (GLUT-1 and GLUT-3) due to abnormally increased glucose metabolism (^{18}F-FDG can be phosphorylated by hexokinase and the product is more polar that can be trapped in the tumor cell, and the cellular concentration of ^{18}F-FDG can be visualized by PET and represent the level of glucose metabolism) (12). Therefore, ^{18}F-FDG PET is widely used in the clinic as a revolutionary imaging technique for tumor diagnosis, staging, treatment planning and prognosis assessment. The diagnostic and prognostic value of ^{18}F-FDG PET in LC patients has been extensively investigated, and studies have also shown the effectiveness of ^{18}F-FDG for NSCLC staging (13–15).

However, since tissue glucose metabolism is not malignancy specific, other conditions, such as inflammatory/infective processes, will also cause increased ^{18}F-FDG uptake and false-positive results (16, 17). Furthermore, a great amount of tumor heterogeneity can be found in all histologic subtypes of LC, and ^{18}F-FDG uptake is variable in different subtypes: SCC displays higher FDG-avid than adenocarcinomas, while pulmonary NETs, lepidic predominant adenocarcinomas and mucinous neoplasms usually show relatively low ^{18}F-FDG uptake (18, 19). Heterogeneity may present in different lesions within the same patient. In addition, multiple microenvironmental factors in different stages of LC, such as hypoxia and tumor angiogenesis, may also affect tumor progression as well as treatment response. Therefore, ^{18}F-FDG PET is not able to provide full information about growth and metabolism of tumors, such as cell proliferation rate, expression of certain receptors, protein synthesis and amino acid metabolism, angiogenesis, etc., and this information are also important for diagnosis and treatment of tumors. To fully investigate tumor features for precise individual treatment, more specific PET radiotracers are required for characterizing tumor pathology and monitoring/predicting the therapeutic response (20).

In past decades, great efforts have been made to develop novel PET tracers to improve the specificity and sensitivity of PET imaging of LC. Although most of these newly reported PET tracers are in the early research stages, several tracers have entered clinical investigations, which hold the unlimited potential of clinical value for diagnostic PET imaging. This paper reviews the recent progress in PET tracers used in LC other than FDG, with their development history, preclinical and clinical results, and potential for future applications.

Imaging of cellular proliferation

Uncontrolled cell proliferation can be found in all subtypes of lung cancer and is regarded as the key prognostic predictor of malignancy. As a ribosomal RNA transcription-related nuclear protein, Ki-67 is highly expressed during the dividing phases of the cell cycle (S, G1, G2, and M), plays a crucial role in cancer metastasis and can be used as a biomarker for the detection of various tumors. Patients with LC who possess high levels of Ki-67 expression are mostly related to poor differentiation, decreased progression-free survival (PFS), and decreased overall survival (OS) (21–23). Studies have shown that ^{18}F-FDG uptake correlates strongly with Ki-67 expression (percentage of positive cells); however, ^{18}F-FDG does not directly target the process of cell proliferation (23–27).

In recent decades, a series of ^{18}F-labeled thymidine analogs, such as ^{18}F-FLT, have been further incorporated into DNA *via* DNA synthesis procedures (^{18}F-FAU, ^{11}C-DST, etc.) (**Figure 1**), were successfully developed as cellular proliferation PET imaging probes. These analogs follow the same salvage pathway as thymidine, in which they were phosphorylated to thymidine monophosphates by upregulated thymidine kinase 1 and hence trapped in cells during S-phase. With these specially designed PET tracers, the cellular proliferating capability of LCs can be directly visualized.

Among these thymidine analogs, ^{18}F-FLT is the most widely used tracer in the clinic. ^{18}F-FLT accumulation in tumor cells correlates with histopathological Ki-67 expression and tumor angiogenesis (28, 29). A study carried out by Buck et al. indicated that 18F-FLT uptake and distribution were related exclusively to malignancies; however, 4 out of 8 benign lesions showed positive ^{18}F-FDG uptake (30). Similar studies were carried out using both ^{18}F-FDG and ^{18}F-FLT thereafter, and the results indicated that ^{18}F-FLT is more specific and more accurate (at least equally) in the detection of primary LC (31, 32). Compared with ^{18}F-FDG, ^{18}F-FLT is more specific and sensitive in the detection of primary tumors but shows less accuracy for N staging in

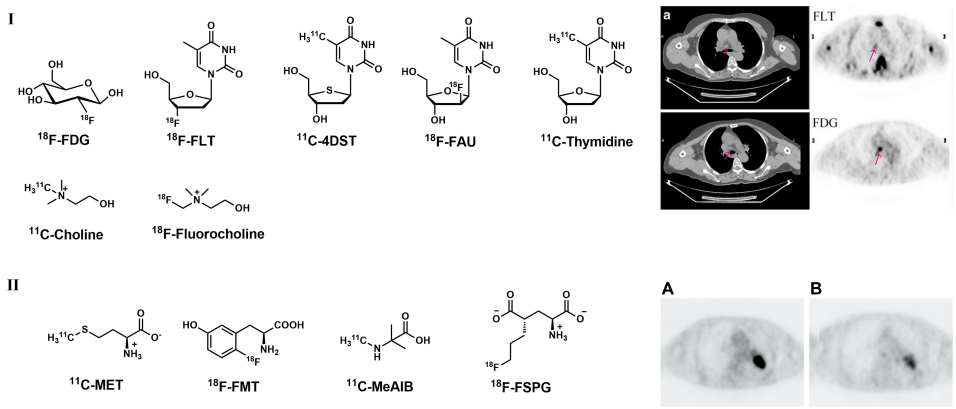

FIGURE 1
Structures of representative PET tracers for cellular proliferation, amino acid metabolism and related representative PET images in LC patient. **(I)** Typical PET and CT images of a 60-year-old patient (female) with adenocarcinoma with ^{18}F-FLT **(upper)** and ^{18}F-FDG **(lower)**; **(II)** ^{18}F-FDG **(A)** and ^{18}F-FMT **(B)** images in 74-year-old patient (male) with lung adenocarcinoma.

LC patients (28, 33, 34). Typical PET images of ^{18}F-FLT in LC patient were presented in **Figure 1** (34).

Trigonis found that a significant decrease in FLT uptake was observed in NSCLC patients (stages I to III) after radiation therapy or radical chemoradiation therapy, which is more sensitive than ^{18}F-FDG (35, 36). Therefore, ^{18}F-FLT shows promising properties in evaluating treatment responses. Furthermore, Kobe et al. found that lower residual ^{18}F-FLT and ^{18}F-FDG uptake were associated with improved PFS in NSCLC patients who had received erlotinib therapy, indicating that ^{18}F-FLT had prognostic value in LC patients (37, 38).

Based on the observations of 4′-methyl-[^{14}C]-thiothymidine with its fast accumulation in rapidly proliferating tissues, ^{11}C-labeled 4′-methyl-thiothymidine (^{11}C-4DST, **Figure 1**) was synthesized and evaluated *in vitro* (39). In a rodent model, ^{11}C-4DST showed high tumor uptake (sensitivity) and selectivity, with a tumor SUV_{max} of 4.93. The tumor-to-muscle ratio is 12.7, which is similar to that of ^{18}F-FDG (13.2) (40). A recent study indicated that ^{11}C-4DST displayed a higher correlation with proliferation of lung cancer, and the correlation coefficient between SUV_{max} and Ki-67 expression was significantly higher with ^{11}C-4DST (0.82) than with ^{18}F-FDG (0.71) in 18 NSCNC patients (41). As an unnatural analog of thymidine, FMAU was first evaluated under clinical investigations for the treatment against hepatitis B virus (HBV) (42). Then, L-FMAU was also radiolabeled with ^{18}F and indicated high tumor uptake in H441 animal models; however, high physiological uptake in the liver and kidneys was investigated in human studies (42, 43).

Although many other radiolabeled thymidine analogs targeting cellular proliferation and DNA synthesis have been reported in recent years, few tracers have entered clinical evaluations. For example, ^{11}C-thymidine (**Figure 1**) showed rapid metabolism and non-specific binding in the bone marrow and liver, indicating that this tracer is not suitable for further clinical use (44). The high concentrations of ^{18}F-FAU in the circulating system and the high activity accumulation in skeletal muscle also limit its application as PET probes (45).

As a quaternary ammonium base, choline is a precursor for the synthesis of cell membrane phospholipids. After phosphorylation, choline is incorporated into phosphatidylcholine and undergoes its metabolic pathway (46). Increased choline metabolism can be observed in oncogenesis and tumor growth processes, as well as tumor proliferation (47). Radiolabeled with ^{11}C or ^{18}F choline analogs have been widely used in PET imaging for the detection of neoplastic tissues (48). ^{11}C/^{18}F-choline (**Figure 1**) showed good performance in many malignant tumors, including LC (48). Although choline analogs usually showed false negatives with low degree of malignancy and highly differentiated neoplasms (49, 50), in solitary lung nodules it was demonstrated that some benign conditions like granulomatous inflammation choline is negative and ^{18}F-FDG is falsely positive. In addition, choline-based PET may be superior to ^{18}F-FDG PET for the diagnosis of granulomatous lymph nodes and lymph node metastasis (49, 51).

Although no relevant guideline has recommended PET imaging of proliferation for diagnosis of tumors, ^{18}F-FLT was the most widely used tracer in clinical investigations and applications.

Imaging of amino acid metabolism and transportation

Beyond glucose, an abundant supply of amino acids is important for cancer cells to sustain their proliferation activities. Amino acids not only play crucial roles in nucleosides and

protein synthesis for the maintenance of cellular homoeostasis but also serve as important suppliers for energy metabolism (52). In most LC malignancies, upregulated amino acid transportation and metabolism can be observed. Therefore, PET imaging of amino acid transport and metabolism showed effectiveness in diagnosing tumors.

As an important intermediate in phospholipidic biosynthesis in lung cancer cells, methionine (MET) can directly reflect amino acid transportation; therefore, ^{11}C-MET (**Figure 1**) can be used as an effective PET tracer for detecting tumors. According to a variety of past studies, ^{11}C-MET PET/CT is more specific and sensitive than ^{18}F-FDG in differentiating benign lesions and lung cancer in pneumoconiosis (53–57). In addition, with the advantage of low physiological uptake in the brain, ^{11}C-MET PET/CT showed better efficacy in detecting LC with brain metastasis (58, 59).

Other radiolabeled amino acids, such as L-[3-^{18}F]-alpha-methyltyrosine (^{18}F-FMT, **Figure 1**) and 2-amino[^{11}C]methyl-isobutyric acid (^{11}C-MeAIB, **Figure 1**), were also developed for the detection of LC in the last decade (60). Mori et al. found that ^{18}F-FMT uptake is related to proliferative activity and tumor angiogenesis in NSCLC and could serve as an independent prognostic factor for patients carrying pulmonary adenocarcinoma (60, 61). ^{18}F-FMT uptake is strongly correlated with amino acid transporter (LAT1) and holds higher specificity in tumors than in peripheral organs, which makes ^{18}F-FMT a promising PET tracer for detecting amino acid transportation in LC (62). In addition, ^{18}F-FMT also showed prognostic value for OS in NSCLC patients according to past research (**Figure 1II**) (63, 64). Nishii et al. found that ^{11}C-MeAIB PET achieved better capability than ^{18}F-FDG in differentiating benign and malignant pulmonary and mediastinal mass lesions and better accuracy than ^{11}C-MET in diagnosing brain tumors (65). As a glutamic acid derivative, ^{18}F-labeled (S)-4-(3- -fluoropropyl)-l-glutamic acid (^{18}F-FSPG, BAY 94-9392, **Figure 1**) also showed promising results in the detection of malignant diseases, including NSCLC (66).

Beyond those tracers, there have been many reports about radiolabeled amino acids targeting protein synthesis and amino transportation pathways, along with their applications in detecting tumors in recent decades, such as ^{18}F-FET, ^{18}F-FACBC, ^{11}C-ACBC, ^{11}C-ACPC ^{11}C-AMT, etc. Those tracers have also been investigated in LC patients in clinic, but the details are not discussed because of the scope of this paper (67–70).

According to the joint European Association of Nuclear Medicine (EANM)/European Association of Neuro-oncology (EANO)/Working group of Response Assessment in Neuro-Oncology (RANO) practice guidelines and Society of Nuclear Medicine and Molecular Imaging (SNMMI) standard procedures, ^{11}C-MET, ^{18}F-FET yielded high-quality imaging standard by PET with patients with glioma as well as ^{18}F-FDG (71).

Imaging of tumor hypoxia

Oxygen is crucial for cellular energy metabolism. However, hypoxia was observed in a variety of solid tumors and was regarded as an important biological feature (72). Hypoxia is also considered to be associated with chemotherapy resistance and radiotherapy resistance. Several studies have shown that imaging assessments of hypoxia may hold great value to select patients who would benefit from individualized targeted therapy utilizing the presence of hypoxia (72). With the help of specially designed radio-labeled tracers, PET imaging of tumor hypoxia may provide non-invasive, repeatable images with high spatial resolution and high sensitivity against hypoxic regions in LC. PET hypoxia tracers can be classified into two groups according to their structures: (1) Radiolabeled nitroimidazole analogs; (2) metal chelates.

Nitroimidazole analogs

Nitroimidazoles can be reduced into reactive intermediary metabolites in the presence of intracellular reductases, and this process is directly regulated by the level of hypoxia. Subsequently, nitroimidazole undergoes a futile reduction cycle and returns to the original structure with sufficient competitive electron acceptors. Otherwise, nitroimidazole compounds will be trapped in the hypoxic cells through the formation of hydroxylamine alkylating agents after a reduction reaction (73). Therefore, this process can be visualized by radiolabeled nitroimidazole compounds via PET imaging.

According to clinical research, tumor hypoxia is highly variable and widely prevalent. ^{18}F-FMISO (**Figure 2**) was first synthesized in 1986 and is now the most widely used derivative of nitroimidazole (74). Kubota et al. discovered increased ^{18}F-FMISO uptake in hypoxic and radioresistant tumors in rat models (75). Then, ^{18}F-FMISO accumulation was found to be well associated with the pO2 measurements in head and neck cancer and renal cell carcinoma (76–79). In preclinical studies, ^{18}F-FMISO PET imaging demonstrated better utility and feasibility to identify tumor hypoxic areas compared with ^{18}F-FDG PET (80–82). A variety of human tumors were evaluated by ^{18}F-FMISO, and the results indicated that hypoxic regions could be effectively visualized within different tumors or different regions in the same tumor. Based on a study carried out with 8 patients bearing advanced NSCLC, ^{18}F-FMISO PET can be used to define the hypoxic subareas that may correspond to the region of local recurrences. Additionally, ^{18}F-FMISO uptake could be estimated as a prognostic factor and was associated with the risk of locoregional failure when used in combination with a hypoxia sensitizer (83–85). These results suggest that ^{18}F-FMISO uptake may be used to predict the response to treatment and OS (86). However, with a partition coefficient (octanol/water) value of 0.44, slow whole-bode clearance and

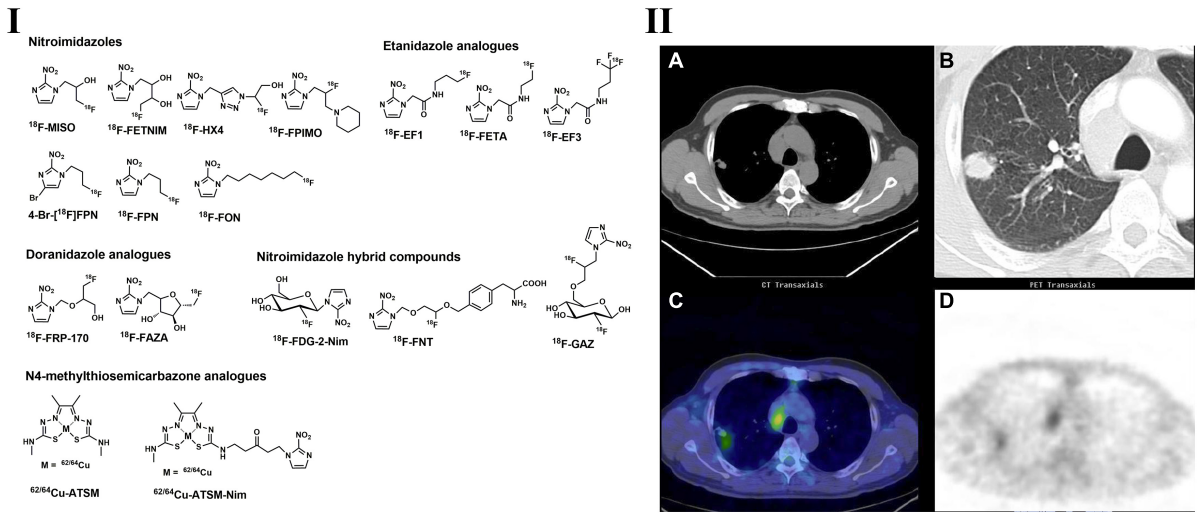

FIGURE 2
Structures of representative PET tracers for tumor hypoxia **(I)** and typical PET and CT images of ^{62}Cu-ATSM in patient with lung adenocarcinoma **(II)**. **(IIA,B)** CT images indicated the mediastinal lymphadenopathy and lung tumor located in right upper lobe; **(IIC,D)** ^{62}Cu-ATSM PET and PET/CT images shows high radioactivity accumulation in the enlarged lymph node and lung tumor.

low contrast of ^{18}F-FMISO PET images were observed, making ^{18}F-FMISO criticized and not favorable for clinical use (72, 87).

Bearing the same scaffold of nitroimidazole, ^{18}F-FETNIM (**Figure 2**) can specifically accumulate in hypoxic cells via the same mechanism as ^{18}F-FMISO. However, ^{18}F-FETNIM is more hydrophilic than ^{18}F-FMISO with two hydroxyl groups and is expected to have faster clearance from well-oxygenated tissues, leading to a higher tumor-to-background (T/B) ratio than 18F-MISO in rodent models (88). In a preclinical study, ^{18}F-FETNIM showed a hypoxia detection capability similar to that of 18F-FMISO in mice bearing C3H mammary carcinoma. Jinming et al. carried out a head-to-head diagnostic evaluation of ^{18}F-FETNIM and ^{18}F-FDG PET imaging in 26 patients with NSCLC. Both ^{18}F-FDG and ^{18}F-FETNIM are beneficial in the clinical evaluation of solid tumors, and 18F-FETNIM provides valuable tumor hypoxia and can be used to predict OS (89). In a study containing 32 patients bearing NSCLC, the radiotherapy response was assessed by ^{18}F-FETNIM PET. They found that high uptake of ^{18}F-FETNIM before radiation therapy correlates with a trend toward poor OS (90). Another study carried out by Lehtiö et al. on ^{18}F-FETNIM PET in head and neck cancer demonstrated similar results (91).

Another nitroimidazole analog bearing a triazole side chain, ^{18}F-HX4 (**Figure 2**), showed high accumulation in tumors and potential in the evaluation of tumor hypoxia. ^{18}F-HX4 demonstrated faster clearance by the kidney and gallbladder and thus allowed a shorter waiting time after the injection of this tracer, making it more convenient for clinical use. The tumor-to-muscle (*T*/*M*) ratio of ^{18}F-HX4 is similar to that of ^{18}F-FMISO in lung cancer patients. A slight increase in the *T*/*M* ratio could be observed as the imaging time was extended. ^{18}F-HX4 showed higher sensitivity and specificity to hypoxia than ^{18}F-MISO and displayed higher signal-to-background contrast, which makes it more suitable for clinical use (92, 93).

To optimize the suboptimal signal-to-background ratio, more hypoxic tracers were thus developed. With the introduction of the sugar moiety, ^{18}F-FAZA (**Figure 2**) has better hydrophilicity than ^{18}F-FMISO and displayed higher tumor-to-muscle ratios (94). In preclinical and clinical studies, ^{18}F-FAZA showed promising accumulation in hypoxic regions and indicated efficient prognostic value (95, 96). Fourteen patients with unresectable lung cancer underwent ^{18}F-FDG and ^{18}F-FAZA PET/CT on consecutive days, ^{18}F-FAZA showed similar tracer uptake with ^{18}F-FDG, and ^{18}F-FAZA uptake in lymph nodes could be used to predict the therapy response in advanced NSCLC patients (97, 98).

Multiple nitroimidazole-based PET tracers have been developed in recent years, such as ^{18}F-FPIMO, ^{18}FPN, ^{18}FON, 4-Br^{18}FPN, ^{18}F-labeled Etanidazole analogs (^{18}F-EF1, ^{18}F-FETA, etc.), ^{18}F-labeled Doranidazole analogs (^{18}F-FRP-170) and nitroimidazole hybrid compounds (^{18}F-FDG-2-Nim, ^{18}F-FNT, and ^{18}F-GAZ) (see **Figure 2**). However, most of them did not show potential superiority to ^{18}F-MISO to be developed as hypoxia PET tracers and need further investigation (99–104).

Metal chelates

The typical metal chelate used in hypoxia PET imaging is radio-copper-labeled diacetyl-bis(N4-methylthiosemicarbazone) (62/64Cu-ATSM) (**Figure 2**) (72, 105). The accumulation of Cu-ATSM is observed in a

redox environment with hypoxia, and several studies suggest that the accumulation is a result of Cu(II) to Cu(I) reduction by NADH/NADPH-based mitochondrial reduction (105). However, the precise mechanism of this tracer for the location trapping in normoxic and hypoxic regions/tissues remains uncertain. ^{64}Cu-ATSM was first found to have significant hypoxia selectivity in EMT6 cells, and the selectivity was further confirmed in animal models such as 9L gliosarcoma, R3327-AT and FaDu human squamous cell rat models (106–109).

Tanaka et al. performed extensive investigations and found that ^{64}Cu-ATSM uptake regions consisted of tumor cells that stayed in the cell cycle and that these cells were quiescent but clonogenic, and the regions were also hypervascular; however, ^{18}F-FDG uptake regions consisted of tumor proliferative tumor cells and were hypervascular (110, 111).

Based on numerous clinical studies, ^{64}Cu-ATSM PET is feasible for the detection of tumor hypoxia, including LC, and may possess prognostic value in anticancer treatments (112–115). Compared with other tumor hypoxia PET tracers, ^{64}Cu-ATSM displayed a higher tumor-to-background ratio and thus provided clearer delineation of tumor regions (116). According to the ^{64}Cu-ATSM PET imaging in patients with locally advanced NSCLC, quantitative and optimal semiquantitative results indicated that hypoxic burden (volume of hypoxic tumor volume * SUV_{mean}) and hypoxic tumor volume had a significant correlation with PFS (progression of free survival) (117).

Although tumor hypoxia was proved to be crucial with tumor therapies, relevant PET tracers have not been implemented in international guidelines and radiolabeled ATSM was the preferred PET tracer in detection of tumor hypoxia in clinical studies and applications.

Imaging of angiogenesis

Angiogenesis is associated with the formation of new blood vessels and other important physiological/pathological processes, including wound repair, physical development, reproduction, response to ischemia, solid tumor growth, and metastatic tumor spread (118). Therefore, angiogenesis has gained attention as a critical imaging target in recent years for the detection of malignant tumors, including LC (119, 120). Multiple factors have been found to be related to the complex and multistep process of angiogenesis, including vascular endothelial growth factor (VEGF), hypoxia-inducible Factor 1 (HIF-1), platelet-derived growth factor (PDGF), transforming growth factor beta (TGF-β), fibroblast growth factor-2 (FGF-2), and angiopoietins (121). Although a variety of factors exist, VEGF is considered the most important and potent factor (122, 123). In addition to those angiogenic factors, integrins have also been involved in a number of physiological/pathological processes associated with angiogenesis, including cell adhesion, differentiation, proliferation, migration, and survival (124). Specifically, as a heterodimeric cell surface receptor, $\alpha_v\beta_3$ integrin plays a crucial role in angiogenesis by allowing the interaction between the cells and extracellular matrix and promoting the migration of endothelial cells. Therefore, VEGF and $\alpha_v\beta_3$ integrin are regarded as the most important targets in multiple molecular imaging studies, including PET (125–127). Hence, currently focused PET tracers for *in vivo* imaging of angiogenesis can be subclassified into the following groups: (1) radiolabeled VEGF pathway inhibitors; (2) radiolabeled integrin antagonists.

Based on the reversible and irreversible binding domains to VEGF tyrosine kinase receptors, monoclonal antibodies (mAbs) displayed improvements in NSCLC patients with treatment response, PFS, and OS. Radiolabeled monoclonal antibodies are effective for the non-invasive imaging of VEGF abundant tumors and prognostic evaluation of VEGF targeted treatment (128). Luo et al. recently reported that PET imaging with ^{64}Cu-NOTA-RamAb provided initial evidence for overexpression of VEGFR-2 in xenografted lung tumors, suggesting potential applications in VEGFR-2-positive lung cancers (129). The VEGF ligand family has several subtypes: VEFG-A, VEFG-B, VEFG-C, VEFG-D, VEGF-E, VEGF-F, and placental growth factor (PIGF). In addition to radiolabeled RamAb, several mAbs that target tumor-associated VEGF ligands were developed as PET tracers and evaluated in preclinical studies and clinical trials. Among those mAbs, ^{86}Y-CHX-A″-DTPA-bevacizumab indicated the highest uptake in VEGF-positive tumors in MSTO-211H, SKOV-3 and LS-174T xenografted mouse models (130). In a recently performed immuno-PET trial containing 7 NSCLC patients, ^{89}Zr-bevacizumab successfully visualized the tumors, and the tumor uptake indicated a positive relationship with PFS and OS (131).

Integrins are cell adhesion molecules in activated tumor endothelial cells and are considered to be involved in the differentiation, growth, migration, and neovascularization of cancer cells. With the core structure of the arginine-glycine-aspartic acid (RGD) sequence, integrin $\alpha_v\beta_3$ binds to various extracellular matrix molecules with high specificity and affinity and plays a crucial role in the regulation of tumor growth, invasiveness and distant metastasis. Therefore, numerous integrin $\alpha_v\beta_3$ agonists and antagonists have been developed as novel PET tracers for imaging angiogenesis (132, 133). In a clinical study with ^{18}F-galacto-RGD (**Figure 3**) and ^{18}F-FDG PET imaging of 18 patients (including 10 NSCLC patients) with primary or metastatic cancer, no significant correlation between SUVs for ^{18}F-galacto-RGD and ^{18}F-FDG for primary/metastatic lesions separately was observed, suggesting the complementary role of RGD-targeted PET beyond ^{18}F-FDG PET (134). Zheng et al. investigated ^{68}Ga-labeled RGD PET tracer in LC patients and found that ^{68}Ga-NOTA-PRGD2 (**Figure 3**) possess higher specificity in the detection of lymph node metastasis in lung malignancies (135, 136). The recent progress of radiochemistry with ^{18}F-fluoride–aluminum complexes led to the development

of ^{18}F-AlF-NOTA-PRGD2(^{18}F-alfatide) (**Figure 3**) with more convenient production than ^{68}Ga-labeled RGD peptides (137). In LC patients, ^{18}F-alfatide PET allows specific imaging of $\alpha_v\beta_3$ expression status with good tumor-to-background contrast and shows other promising imaging properties (137, 138). Luan et al. evaluated ^{18}F-alfatide in advanced NSCLC patients before and after concurrent chemoradiotherapy (CCRT) and found that in non-responders, the SUV_{max} and T/NT were higher than those in responders, while the uptake ratios of tumor to normal lung could be regarded as an independent predictive factor of short-term results for CCRT in advanced NSCLC patients (139).

Although there have been plenty of PET tracers for the imaging of tumor angiogenesis reported and wildly used in clinical in recent years, none of which have been implemented in international guidelines, in spite of these tracers possess great potential in detecting EGFR status *in vivo* and personalizing therapies for NSCLC patients.

Imaging of pulmonary neuroendocrine tumors

Pulmonary NETs are a heterogeneous subgroup of malignancies that develop from a type of enterochromaffin cell named Kulchitsky cells, including low grade (typical carcinoid tumor), intermediate grade (atypical carcinoid tumor), and high-grade malignant tumors (including small cell lung cancer and large cell neuroendocrine carcinoma) (140, 141). Although high-grade pulmonary NETs tend to have FDG activity, the value of ^{18}F-FDG PET for the assessment of NETs is limited (142, 143). The development of somatostatin receptor (SSTR)-based PET tracers has significantly improved the diagnosis of NETs, including LC. For example, ^{68}Ga-DOTA-TATE, ^{68}Ga-DOTA-TOC, and ^{68}Ga-DOTA-NOC (**Figure 4**) showed specific binding to subtype 2 of SSTR (144). DOTA-NOC also displayed good affinities for subtypes 3 and 5 of SSTR. PET imaging with ^{68}Ga–DOTA peptides offers multiple advantages compared with ^{111}In–pentetreotide-based scintigraphy or SPECT, such as higher affinity to SSTRs and superior contrast and resolution, making ^{68}Ga–DOTA peptides superior and convenient in the diagnosis of gastroenteropancreatic and pulmonary neuroendocrine tumors (144, 145). According to Venkitaraman et al., the specificity, sensitivity, and accuracy of ^{68}Ga-DOTA-TOC PET/CT are higher than those of ^{18}F-FDG PET/CT based on a prospective study with 32 patients (bronchopulmonary carcinoid suspected) (146). In a study for the detection of indeterminate pulmonary nodules, ^{68}Ga-DOTATATE showed more specificity than ^{18}F-FDG (147). In addition, incorporating ^{68}Ga–DOTA-peptide PET imaging into ^{18}F-FDG PET could enhance the specificity and sensitivity for the diagnosis of pulmonary tumors (148–150). Furthermore, indolent tumors showed low FDG uptake but high 68Ga-DOTA-TATE accumulation, indicating the diagnostic value of ^{68}Ga–DOTA-peptides in the evaluation of pulmonary NETs (148).

Moreover, Zhu et al. evaluated the somatostatin receptor (SSTR) and integrin $\alpha_v\beta_3$ dual-target PET tracer (NOTA-3P-TATE-RGD, **Figure 4**) in 32 patients (18 with NSCLC and 14 with SCLC). ^{68}Ga-NOTA-3P-TATE-RGD showed higher uptake than ^{68}Ga-NOTA-TATE in NSCLC patients, with strongly positive $\alpha_v\beta_3$ and moderately positive SSTR2A expression detected by immunohistochemical staining. Furthermore, ^{68}Ga-NOTA-3P-TATE-RGD uptake is also significantly higher than ^{68}Ga-NOTA-RGD uptake in SCLC patients, with strongly positive SSTR2A and negative to mildly $\alpha_v\beta_3$ expression (151, 152).

In addition to somatostatin analogs, radio-labeled SSTR antagonists also showed selective affinity in preclinical and clinical studies (lower affinity than that of DOTA-TATE). Compared with ^{64}Cu-DOTA-TATE, ^{64}Cu-NODAGA-JR11 showed much less internalization but highly strong receptor-mediated accumulation at the cell membrane (153). Specific tumor uptake of ^{64}Cu-NODAGA-JR11 was also confirmed by the co-injection of unlabeled peptide (153). As indicated by a comparison study, Al^{18}F-NOTA-JR11 showed superior imaging quality than ^{68}Ga-DOTA-TATE in HEK293-SSTR2 tumor-bearing mice (154). Huo et al. also compared ^{68}Ga-DOTA-JR11 with ^{68}Ga-DOTA-TATE in patients with neuroendocrine tumors. The results indicate that although ^{68}Ga-DOTA-TATE is better in the diagnosis of bone metastases, ^{68}Ga-DOTA-JR11 (**Figure 4**) showed superior properties in the detection of liver metastases (155).

As an endogenous neurotransmitter, dihydroxy phenylalanine (DOPA) was labeled with ^{18}F and used in the evaluation of the dopaminergic nervous system, as well as the detection of malignancies, including neural crest-derived (neuroendocrine) neoplasms, brain tumors and carcinoid tumors (156–159). DOPA may also accumulate in NETs because it is the substrate of dihydroxyphenol-alanine decarboxylase, which is overexpressed in NETs (160). Therefore, ^{18}F-DOPA (**Figure 4**) PET was also used in the characterization of pulmonary nodules with neuroendocrine activities (161). However, ^{18}F-DOPA showed inferior properties in detecting and staging NETs than ^{68}Ga-DOTA-TATE in a comparative study performed in 25 patients (6 LC patients included) (162). This may explain why few articles could be found with ^{18}F-DOPA PET used in pulmonary NETs.

Among all NET PET tracers, DOTA-TOC/NOC/TATE are the preferred PET Tracer in NET imaging as suggested by European Society for Medical Oncology (ESMO) guideline and have been widely used in clinical for the diagnosis of NETs. ^{18}F-DOPA was wildly used in the diagnosis of Parkinson's disease, and was also recommend for the imaging of glioma as a radiolabeled amino acid by EANM/EANO/RANO guidelines and SNMMI standard procedures (71).

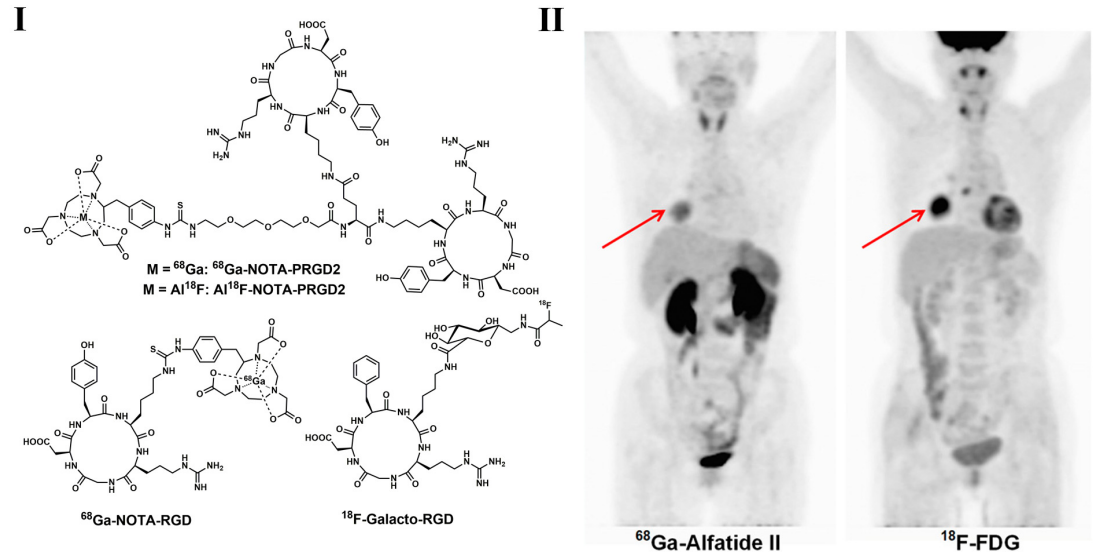

FIGURE 3
Structures of representative angiogenesis PET tracers **(I)** and PET images of ^{68}Ga-Alfatide **(II)** (^{68}Ga-NOTA-PRGD2) and ^{18}F-FDG in patient with representative squamous carcinoma **(II)**.

Imaging of tyrosine kinases in lung cancer patients

Receptor tyrosine kinases (RTKs) are transmembrane receptors in signaling pathways and play crucial roles in the tumorigenesis and pathogenesis of malignant lung cancer. RTKs are key regulators of cancer cell proliferation, differentiation, invasion, metastasis, and angiogenesis. Therefore, RTKs are also regarded as one of the most important targets for tumor treatment (163, 164). With developments in the molecular genotyping of LC (especially NSCLC), more than 50 tumor-associated RTKs have been identified, such as EGFR, c-MET, ROS1, RET, and ALK. A variety of RTK-targeting mAbs and small molecules of tyrosine kinase inhibitors (TKIs) have been developed and demonstrated inspiring clinical outcomes in patients with mutated RTKs. However, an effective patient screening and therapy prediction method is strongly required for individually targeted therapy. With radiolabeled TKIs and mAbs, visualization and quantification of tumor-specific targets become possible with PET imaging. At present, typical radiotracers that target RTKs used in LC can be subclassified into the following categories: (1) EGFR-targeted mAbs and inhibitors; (2) C-MET-targeted inhibitors; (3) VEGF-targeted mAbs and inhibitors. As VEGF is mostly associated with angiogenesis, VEGF-targeted PET tracers are discussed above.

Based on epidemiological findings, NSCLC comprises approximately 80% of all LCs and approximately 60% of NSCLC patients carrying activated EGFR (1, 3, 165). Therefore, EGFR was supposed to be one of the most important targets for *in vivo* imaging of LC. As IgG1 antibodies directed against EGFR, panitumumab and cetuximab were labeled with ^{64}Cu, ^{86}Y, and ^{89}Zr to evaluate the imaging capability in rodent models. According to these preclinical studies, radiolabeled mAbs were found to significantly accumulate in EGFR-expressing tumors with a positive correlation with EGFR levels (166–169). ^{89}Zr-cetuximab was first evaluated in 9 patients (3 head and neck cancer patients and 6 NSCLC patients), and heterogeneous uptake was observed in tumors; therefore, the predictive value of this tracer was not discussed (170). Another study containing 10 colorectal cancer patients was carried out soon. Those patients received co-injection of cold cetuximab and ^{89}Zr-cetuximab and were investigated with 6 serial PET scans; 6 patients displayed increased ^{89}Zr-cetuximab uptake, and 4 of these patients experienced better outcomes after cetuximab treatment. These results indicate that ^{89}Zr-cetuximab PET may not only be used in the detection of EGFR *in vivo* but also be used to predict the response to cetuximab therapy (171).

During the last decade, radiolabeled small molecule EGFR-TKI probes have been extensively investigated in preclinical and clinical studies. As a reversible EGFR TKI, PD153035 and its analogs were labeled with ^{11}C and ^{18}F and evaluated *in vitro* and *in vivo*. ^{11}C- PD153035 (**Figure 5**) showed increased uptake in EGFR-sensitive tumors in rodent models (172, 173). In a subsequent clinical study with 21 patients with advanced chemotherapy-refractory NSCLC, Meng et al. evaluated the potential of ^{11}C-PD153035 for selecting patients who were likely to respond to erlotinib treatment (174). Enhanced ^{11}C-PD153035 uptake in tumors prior to erlotinib treatment correlated positively with longer PFS and better OS. However, the less well-correlated survival indicated that it was not an

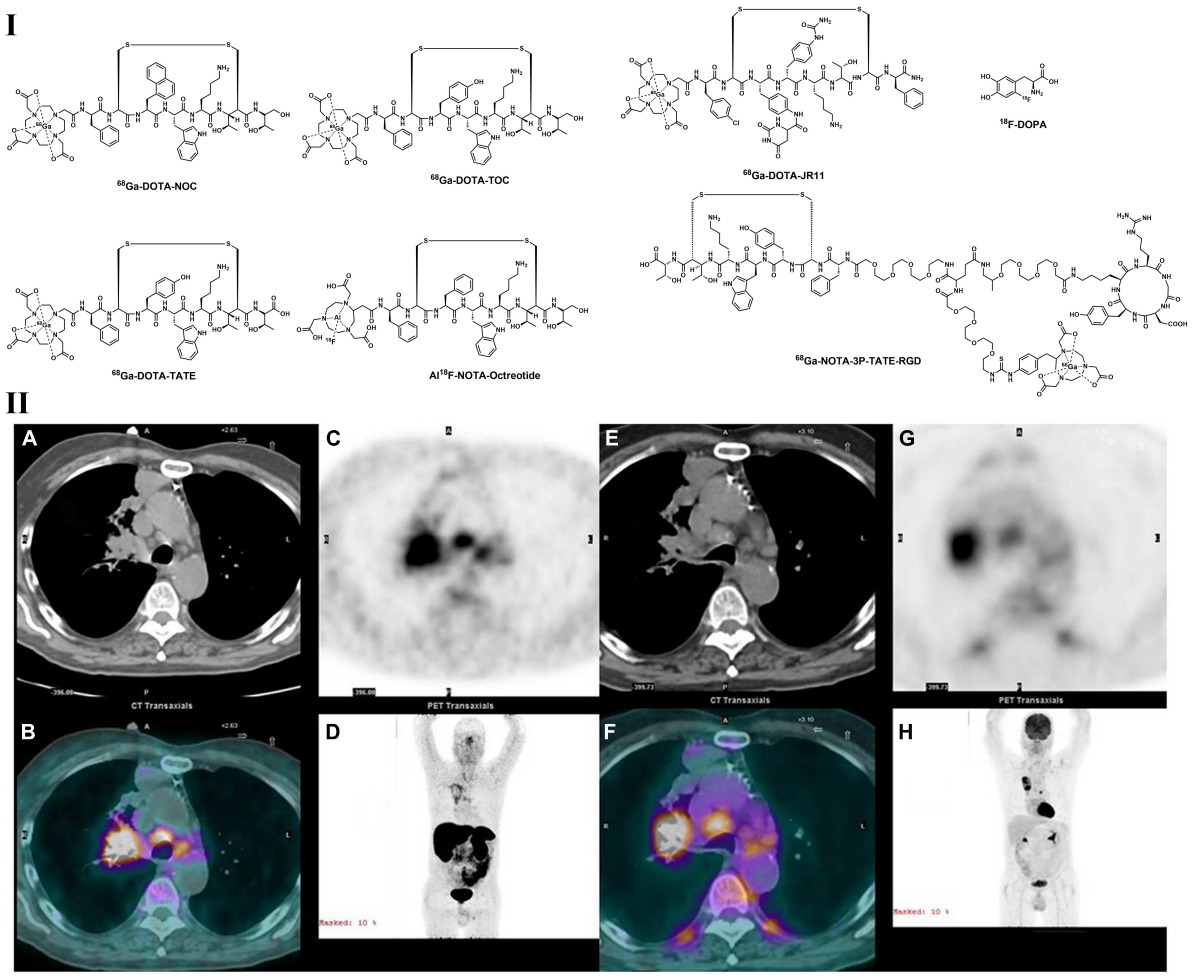

FIGURE 4
Structures of representative PET tracers for pulmonary NETs **(I)** and PET images of ^{68}Ga-DOTATATE **(A–D)** and ^{18}F-FDG **(E–H)** in patient with squamous cell carcinoma **(II)**. Concordant radioactivity accumulation can be observed in mediastinal adenopathy, right hilum and right upper lobe tumor.

ideal prognostic method for EGFR-TKI targeting treatment. As a successful first-generation EGFR-TKI, erlotinib was labeled with ^{11}C (**Figure 5**) and evaluated in a variety of preclinical studies (175). All preclinical studies displayed noticeable uptake in EGFR-sensitive tumors in mice with NSCLC xenograft models, and this uptake can be effectively blocked by the cold erlotinib, suggesting the specifically saturable binding of this tracer. Memon et al. performed the first clinical study using ^{11}C-erlotinib in 13 NSCLC patients, and compared with ^{18}F-FDG, increased uptake of ^{11}C-erlotinib can be observed in malignant lymph nodes and tumors (176).

They also found that ^{11}C-erlotinib showed good blood–brain-barrier penetrability and hence is beneficial for NSCLC patients with brain metastases (177). According to a tracer pharmacokinetic analysis using the distribution volume (V_T) as an uptake parameter, a 2-tissue reversible compartment model best fit ^{11}C-erlotinib (178). Compared with wild-type tumors, the VT of ^{11}C-erlotinib is higher in patients with EGFR exon 19 deletion, indicating that it is sensitive to EGFR mutation (179). Afatinib, a second-generation TKI that irreversibly binds to EGFR, was also labeled with ^{18}F and investigated. Slobbe et al. found that ^{18}F-afatinib (**Figure 5**) was sensitive to tumors with activated EGFR mutations in xenografted mouse models (180). ^{18}F-afatinib showed higher tumor-to-background ratios in EGFR^{19del} and EGFR^{WT} tumors, as well as higher stability in plasma, making this tracer more promising in clinical applications (181). As many radiolabeled EGFR TKIs with a 4-anilinoquinazoline scaffold displayed potent *in vitro* activities but showed inferior imaging properties, such as high non-specific binding, low *in vivo* stability and rapid dissociation rates, structural modifications to this scaffold were thus performed to overcome these issues, and several PET tracers were developed, such as ^{18}F-PEG6-IPQA, ^{124}I-morpholino-IPQA and ^{18}F-MPG (**Figure 5**) (182–184). These

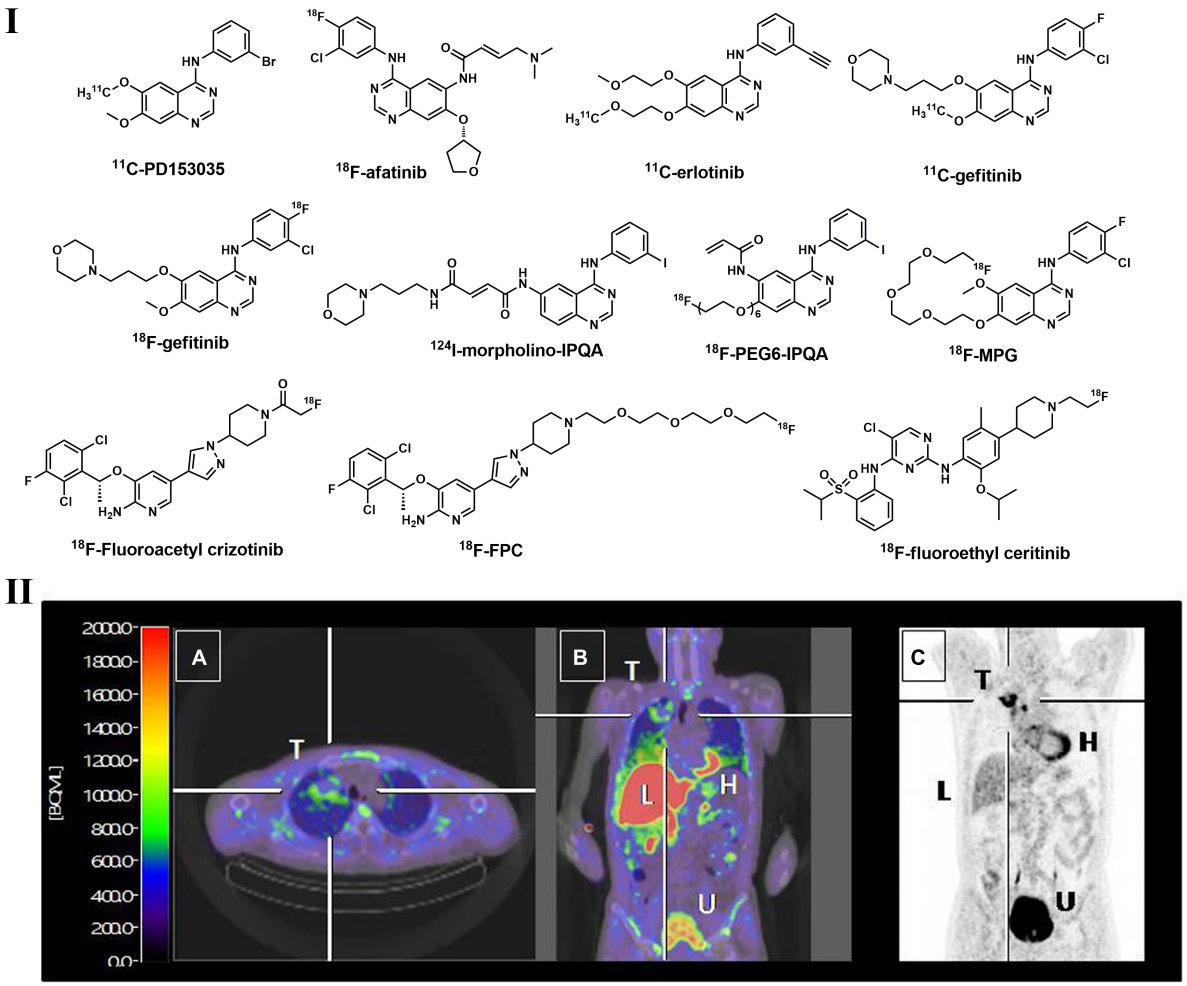

FIGURE 5
Structures of representative radiolabeled TKIs used in lung cancer imaging **(I)** and PET images of ^{18}F-afatinib in a NSCLC patient with EGFR^{19_del} **(II)**. Tumor with EGFR^{19_del} can be clearly visualized by ^{18}F_afatinib (T: tumor; H: heart; L: liver; U: urinary bladder).

tracers also displayed better uptake in tumors with EGFR mutation and lower background noise in both preclinical and clinical investigations.

In addition to the TKI PET tracers described above, several novel TKIs were radiolabeled and evaluated. However, most of them displayed inferior imaging qualities and/or were not capable of distinguishing TKI-sensitive and TKI-resistant tumors, such as ^{18}F-gefitinib, which may be due to their high lipophilicity and limited tumor uptake resulting from other mechanisms (185). Overall, TKI-based PET is an important diagnostic tool for EGFR-positive lung tumors and effective clinical assessment to select those patients who would benefit more from EGFR-TKI-targeted treatment.

The ALK and HGF/c-MET pathways play significant roles in the occurrence and progression of NSCLC, indicating that these targets can be used for diagnosis and therapeutic purposes (186, 187). Accounting for approximately 5–22% of LC, c-MET-positive NSCLC patients are an important subgroup that is resistant to first- or second-generation EGFR TKIs (188). In addition, ALK-rearranged NSCLC patients comprise nearly 5–6% of all NSCLC cases (189). Studies revealed that the survival time of patients with activated c-MET mutation is shorter, suggesting that c-MET positive mutation is an adverse prognostic factor (190). Thus, c-MET-TKI/ALK-based PET imaging assessment has rapidly developed in recent years. As a potent and promising c-MET/ALK dual inhibitor, crizotinib and its analog were labeled with ^{18}F for *in vivo* imaging of c-MET/ALK status (191, 192). According to Manning et al., ^{18}F-fluoroacetyl crizotinib (**Figure 5**) showed selective binding to ALK kinase (H3122 lung cancer cells) *in vitro* (191). A polyethylene glycol (PEG)–modified crizotinib derivative (^{18}F-FPC, **Figure 5**) was synthesized by Cheng et al. and evaluated in c-MET-positive (H1399 cell) and negative (A549 cell) NSCLC rodent models (192). Significant ^{18}F-FPC

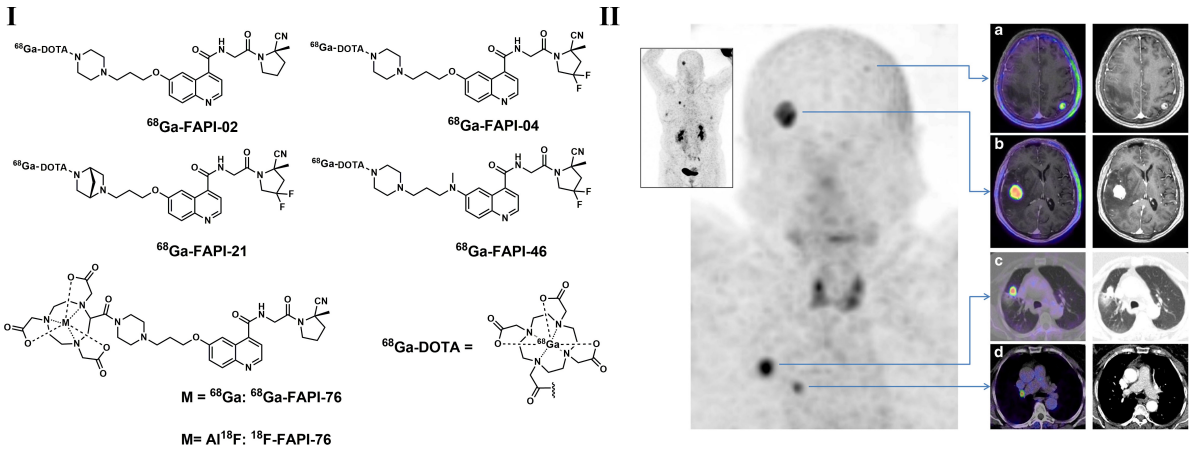

FIGURE 6
Structures of typical radiolabeled FAP inhibitors **(I)** and PET/CT images of ^{68}Ga-FAPI-04 **(a–d)** in a lung cancer patient with brain metastasis **(II)**.

accumulation in H1399 tumors was observed, indicating its potential to distinguish c-MET-positive tumors in NSCLC patients. Perera et al. synthesized ^{18}F-fluoroethyl-ceritinib (**Figure 5**) for the evaluation of ALK expression in solid malignancies, but no *in vitro* or *in vivo* results were reported (193).

Great attention has been paid to RTK-based PET tracers as the development of RTK therapies in the last decades and over 20 PET tracers were reported and evaluated in NSCLC patients, but even the most promising tracers were still under clinical investigations and none of them have been widely accepted in clinical practices.

Imaging of cancer-associated fibroblasts

Cancer-associated fibroblasts (CAFs) have been proved to play important roles in several different properties of cancerous tumors, such as metastasis, migration, immunosuppression, and resistance to chemotherapy (194). Therefore, targeting CAFs may be a useful method for both diagnosis and treatment purposes. As a type II transmembrane protein expressed in activated fibroblasts, fibroblast activation protein (FAP) is highly overexpressed in a variety of malignant tumors and is related to poor prognosis, indicating that FAP is a potential target for PET imaging (195, 196). FAP imaging has been carried out with antibodies and small molecular inhibitors during the last decade (194). Several initial FAP-targeted tracers were not focused on tumor imaging; for example, radioiodine-labeled MIP-1232 was used in the detection of atherosclerotic plaques, and ^{111} In-, ^{89} Zr-, or ^{99m}Tc-labeled antibody 28H1 was used for the imaging of rheumatoid arthritis. However, based on the structural modification of a quinoline-based FAP inhibitor and DOTA as chelator, a series of small molecule FAP PET tracers (^{68}Ga-FAPIs, **Figure 6**) were developed and evaluated in recent years. With relatively lower lipophilicity, ^{68}Ga-FAPIs showed fast body clearance and high uptake in malignant tissues according to biodistribution studies, resulting in promising high tumor-to-background images. Based on a PET imaging study in NSCLC patients, accumulated radio-labeled FAPI signals were observed not only in tumor lesions but also in active tissue remodeling sites, such as arthritis, chronic inflammation and physiological uptake in the uterus (194, 197). ^{68}Ga-FAPI-04 and ^{68}Ga-FAPI-46 showed the best activity against FAP and superior pharmacokinetic profiles among all reported tracers (198). According to Giesel et al., extremely high ^{68}Ga-FAPI-04 uptake was found in 28 kinds of tumors, including NSCLC. FAPI was also radiolabeled with ^{18}F via NOTA as a chelator to prepare ^{18}F-FAPI-74. It also showed ideal imaging quality and even a lower radiation burden than ^{68}Ga-FAPI-74, making FAPI-74 more flexible for clinical applications in LC (199, 200). Overall, coupling highly selective FAPIs to DOTA or other chelators, such as NOTA, FAP-targeted imaging with ^{68}Ga or treatment with other therapeutic isotopes can be achieved (201).

Imaging of other targets

In addition to the changes in the tumor microenvironment and special physiological/pathological processes described above, several other activated systems, signaling pathways and key proteins that led to the development of LC were also regarded as important targets for the discovery of novel PET tracers. These tracers have been reported for the imaging of LC and provide valuable information on target abundance and hence can be used in the determination of personalized treatment plans, as well as the prediction of therapeutic

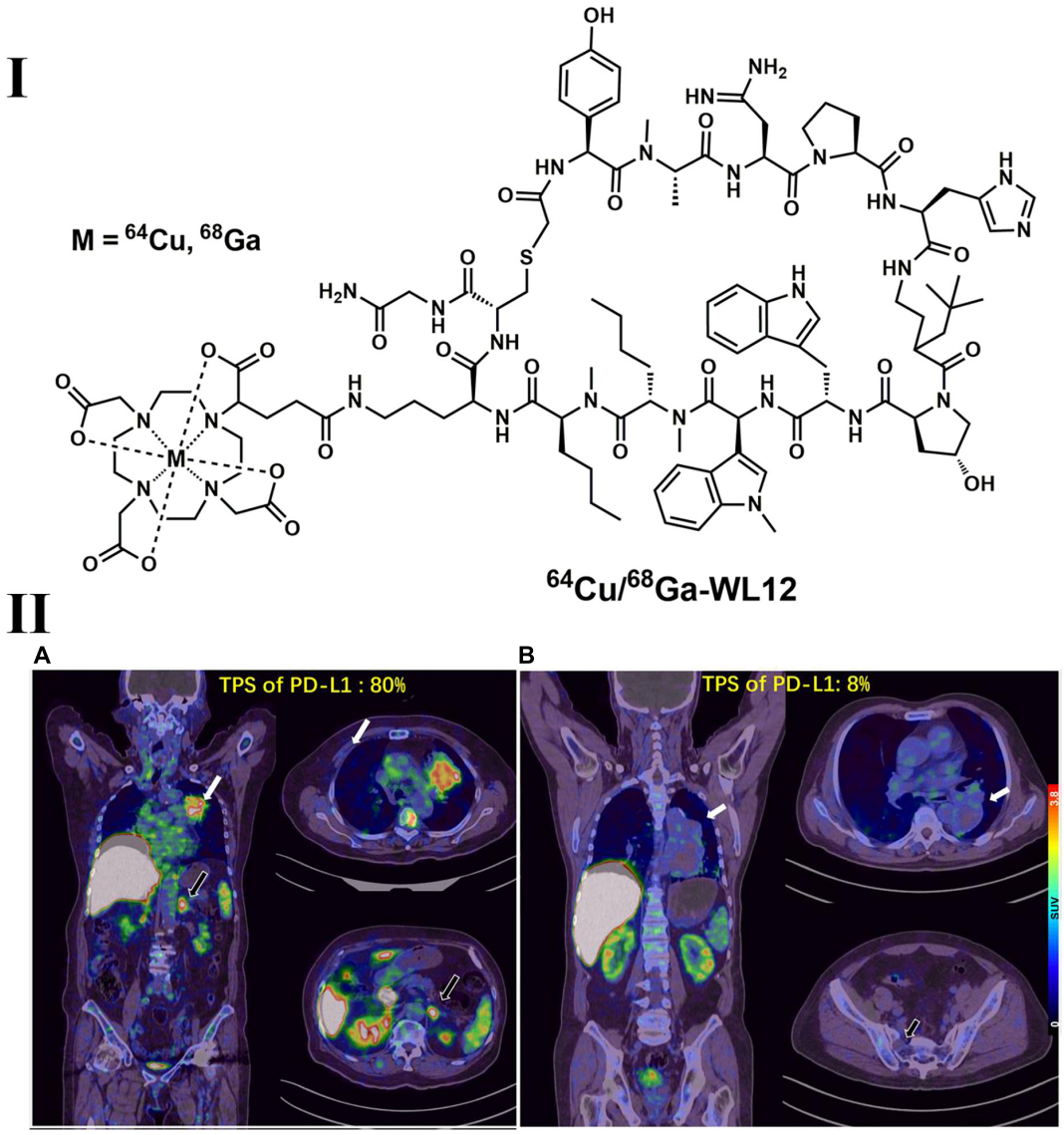

FIGURE 7
Structure of ^{64}Cu/^{68}Ga-WL12 **(I)** and representative PET images of ^{68}Ga-WL12 in patients with NSCLC **(II)**. **(IIA)** An 80-year-old patient (female) with advanced NSCLC and a PD-L1 TPS value of 80%; **(IIB)** a 68-year-old patient (male) with a PD-L1 TPS value of 8%.

response. Several successfully developed PET tracers based on these targets used in LC patients have been reported in recent years and are briefly described in this section.

Imaging of programmed cell death pathways

As a revolutionary cancer therapy that produces durable responses, immuno-oncology-based immune checkpoint therapy benefits patients with a variety of malignant tumors, including LC (202). Approximately 20% of NSCLC patients have achieved tumor responses when treated with immune checkpoint inhibitors. The expression of PD-1 in tumor-infiltrating lymphocytes and PD-L1/CTLA4 in the tumor cell membrane may be predictive for the response to immune checkpoint therapies. Natarajan et al. synthesized ^{64}Cu-DOTA-(anti-mouse)-PD1 and evaluated it in mice xenografted with melanoma tumor cells (203). High tracer uptake was observed in tumors and lymphoid organs. The specific binding of the tracer was confirmed by bioluminescence imaging and self-blocking experiments. Ring et al. synthesized a radio-labeled PD-1 antibody named ^{64}Cu–DOTA–HAC and evaluated it in mouse xenograft tumor models. ^{64}Cu–DOTA–HAC showed

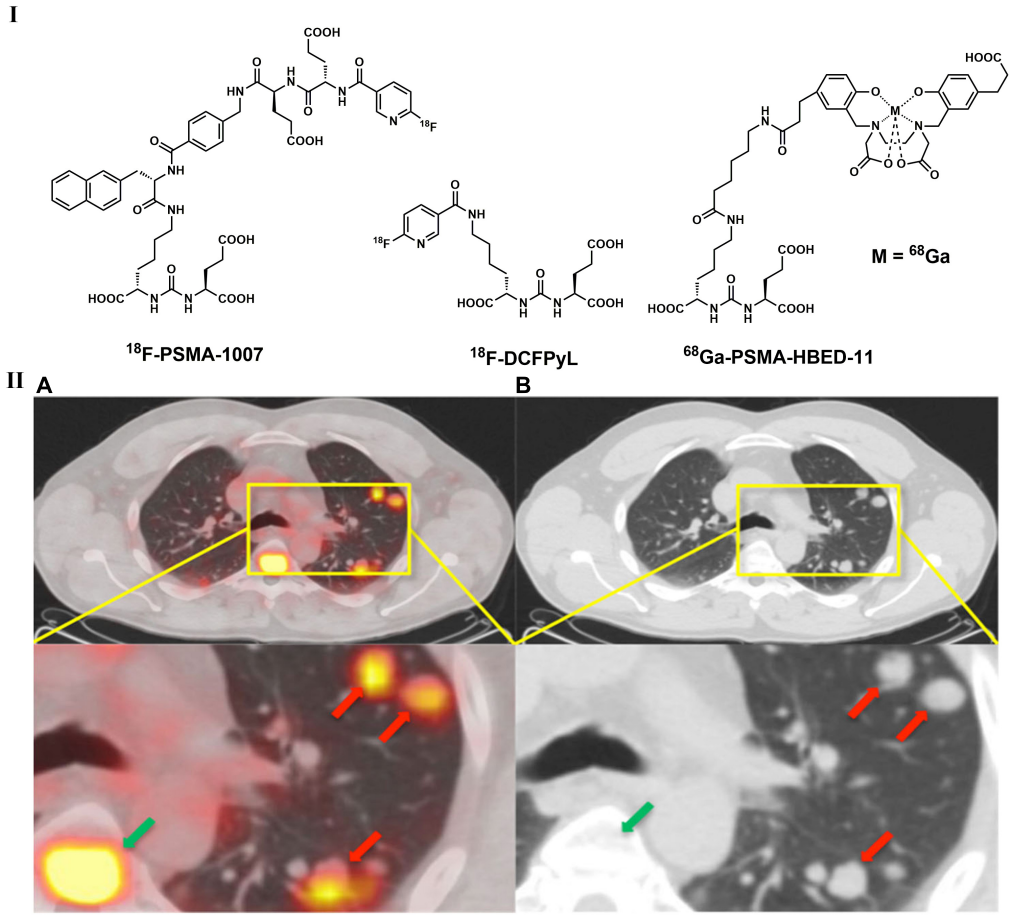

FIGURE 8
Structures of representative PSMA-targeted PET tracers **(I)** and PET/CT **(A)** and unenhanced CT **(B)** images of ^{68}Ga-PSMA-HBED-11 in patient with with a recurrent prostate acinar adenocarcinoma and lung metastases **(II)**.

higher tracer up in hPDL1-positive tumors compared with hPDL1-negative tumors, providing an alternative method to invasive histological and biopsy analysis to distinguish between PD-L1–positive from PD-L1–negative tumors *in vivo* (204). Yang et al. prepared ^{64}Cu-NOTA-αCD276/Fab, and this probe was used in the evaluation of a CD276-targeted photodynamic therapy in NSCLC mouse models, as well as other imaging modalities for the detection of its efficacy in enhancing anti-PD-1/PD-L1 cancer therapies (205). Based on a single-domain antibody, Lin et al. synthesized a ^{68}Ga-labeled PET tracer through a NOTA chelator named ^{68}Ga-NOTA-Nb109 (206). According to biodistribution, autoradiography, PET imaging and immunohistochemical staining studies, ^{68}Ga-NOTA-Nb109 showed specific accumulation in A375-hPD-L1 tumors with an uptake ratio of 5.0 5.0% ± 0.35% at 1 h postinjection.

In addition, a series of peptide-based imaging agents, such as ^{68}Ga-WL12, ^{64}Cu-WL12 (**Figure 7**) and ^{18}F-FPy-WL12, with high affinity (IC_{50} = 23 nM for WL12 and 26–32 nM for FPy-WL12, respectively) were synthesized and evaluated in mice bearing cancer xenografts. The results indicated that both ^{68}Ga-WL12 and ^{18}F-FPy-WL12 showed high tumor uptake in PD-L1-positive tumors (including NSCLC), and the uptake could be blocked by the injection of cold reference standards (207–209). Furthermore, ^{68}Ga-NOTA-WL12 was recently evaluated in 9 NSCLC patients (210). After the baseline scan of ^{68}Ga-NOTA-WL12 and ^{18}F-FDG dual PET imaging, patients also received a combination of chemotherapy and pembrolizumab, and follow-up dual PET imaging was also performed. High contrast tumor images were obtained in ^{68}Ga-NOTA-WL12 PET with tumor-to-lung ratios of 4.45 ± 1.89 at 1 h, and a strong correlation between PD-L1 expression and tracer uptake was observed, indicating potential benefits of this tracer used in clinical PD-L1 therapy (210). Although not all PD-1- and PD-L1-targeted PET tracers have been evaluated in NSCLC tumor models or patients, the significant progress in clinical outcomes achieved by anti-PD-1/PD-L1 treatments in advanced NSCLC patients will undoubtedly promote the applications of these tracers in NSCLC patients.

Imaging of prostate-specific membrane antigen

As a type II transmembrane protein, prostate-specific membrane antigen (PSMA) possesses glutamate carboxypeptidase/folate hydrolase activity and is a promising target for prostate cancer imaging (211, 212). A variety of radiolabeled PSMA ligands, such as ^{68}Ga-PSMA-11 (**Figure 8**), were introduced for PET imaging, and β radionuclide ^{177}Lu conjugated drugs were developed for therapy thereafter (213, 214). PSMA-targeted PET imaging and radiopharmaceutical therapy have enabled significant prostate-specific antigen imaging and therapeutic responses (215). Notably, increased ^{68}Ga-PSMA uptake was not only observed in prostate cancer lesions but also found in several other benign and malignant lesions (216). According to Schmidt et al., approximately 6% of NSCLC cells express PSMA, which was mainly discovered in squamous cell carcinoma (217). In addition, the one who was diagnosed with confirmed prostate cancer had intense uptake of ^{68}Ga-PSMA in lung nodules (218). Although it is not possible to easily distinguish prostate cancer lung metastases from primary lung cancers, PSMA-based PET imaging still supplies a method to seek primary tumors in the lung (217, 219, 220). By incorporating the Lys-urea-Glu motif, a variety of radiolabeled PSMA ligands (**Figure 8**) have been discovered in recent years, including ^{11}C-MCG, ^{18}F-DCFBC, ^{18}F-DCFPyL, and ^{18}F-PSMA-1007 (214, 215). Several studies have suggested that radiolabeled PSMA ligands can be used in the detection of prostate cancer with lung metastases, but further investigations are needed (219, 221). It is interesting that intense uptake of ^{68}Ga-PSMA-11 in lung nodules was found in a male patient (diagnosed with prostate cancer), but no significant uptake of ^{18}F-FDG was observed (218). Although it is not possible to easily distinguish prostate cancer lung metastases from inflammatory conditions and primary lung cancers, PSMA overexpression in LC could expand the diagnostic applications of PSMA-based PET in the clinic (217, 219, 220). In addition, ^{68}Ga-PSMA-11 have been implemented in the NCCN (222).

Conclusion

As a unique imaging modality and clinical assessment, PET/CT allows the *in vivo* detection and quantitative analysis of the desired target, as well as physiological/pathological processes at the molecular level. Although ^{18}F-FDG showed high sensitivity and has been widely used in the detection, staging/restaging, treatment planning and prognosis evaluation in LC patients, a variety of other types of PET tracers were developed to investigate different aspects of the cancer microenvironment and biology and to improve tumor characterization, patient stratification, treatment response assessment and therapeutic response monitoring. These new tracers are used for the imaging of cellular proliferation, amino acid metabolism and transportation, tumor hypoxia, pulmonary NETs and special targets in LC. Although most tracers have shown promising qualities in preclinical studies, their clinical applications are limited. As the targets described above are not lung cancer specific, these tracers are also not specific to lung lesions, and not all tracers described above have been used for the detection of lung lesions. As a large number of tracers and related research articles have been reported in recent decades, not all tracers and valuable articles were included due to the scope of this paper.

With the development of targeted PET imaging and targeted therapies, more PET tracers that target specific targets, signaling pathways and tumor biology will definitely play increasingly important roles in routine clinical practice.

Author contributions

HF, XW, and LL designed this study. YLL, HC, and YCL collected the data. JZ, FP, and LP drafted the manuscript. All authors revised this manuscript and approved for submission.

Funding

This study was supported by college subject of Mianyang Central Hospital (No. 2020FH02), Sichuan Science and Technology Program (No. 2020YFS0572), post-doctor research project, West China Hospital, Sichuan University (2020HXBH046), NHC Key Laboratory of Nuclear Technology Medical Transformation (MIANYANG CENTRAL HOSPITAL, Grant No. 2021HYX002), and 1.3.5 project for disciplines of excellence, West China Hospital, Sichuan University (ZYGD18016 and ZYJC21071).

Conflict of interest

The authors declare that the research was conducted in the absence of any commercial or financial relationships that could be construed as a potential conflict of interest.

Publisher's note

References

1. Ferlay J, Colombet M, Soerjomataram I, Dyba T, Randi G, Bettio M, et al. Cancer incidence and mortality patterns in Europe: Estimates for 40 countries and 25 major cancers in 2018. *Eur J Cancer.* (2018) 103:356–87. doi: 10.1016/j.ejca.2018.07.005

2. Duma N, Santana-Davila R, Molina JR. Non-Small cell lung cancer: epidemiology, screening, diagnosis, and treatment. *Mayo Clin Proc.* (2019) 94:1623–40. doi: 10.1016/j.mayocp.2019.01.013

3. Brennan P, Hainaut P, Boffetta P. Genetics of lung-cancer susceptibility. *Lancet Oncol.* (2011) 12:399–408. doi: 10.1016/s1470-2045(10)70126-1

4. Jamal-Hanjani M, Wilson GA, McGranahan N, Birkbak NJ, Watkins TBK, Veeriah S, et al. Tracking the evolution of non-small-cell lung cancer. *N Engl J Med.* (2017) 376:2109–21. doi: 10.1056/NEJMoa1616288

5. Langer CJ, Besse B, Gualberto A, Brambilla E, Soria JC. The evolving role of histology in the management of advanced non-small-cell lung cancer. *J Clin Oncol.* (2010) 28:5311–20. doi: 10.1200/jco.2010.28.8126

6. Sant M, Allemani C, Santaquilani M, Knijn A, Marchesi F, Capocaccia R. EUROCARE-4. Survival of cancer patients diagnosed in 1995-1999. Results and commentary. *Eur J Cancer.* (2009) 45:931–91. doi: 10.1016/j.ejca.2008.11.018

7. Saif MW, Tzannou I, Makrilia N, Syrigos K. Role and cost effectiveness of PET/CT in management of patients with cancer. *Yale J Biol Med.* (2010) 83:53–65.

8. Akhurst T. Staging of non-small-cell lung cancer. *PET Clin.* (2018) 13:1–10. doi: 10.1016/j.cpet.2017.09.004

9. Ambrosini V, Nicolini S, Caroli P, Nanni C, Massaro A, Marzola MC, et al. PET/CT imaging in different types of lung cancer: an overview. *Eur J Radiol.* (2012) 81:988–1001. doi: 10.1016/j.ejrad.2011.03.020

10. Cremonesi M, Gilardi L, Ferrari ME, Piperno G, Travaini LL, Timmerman R, et al. Role of interim (18)F-FDG-PET/CT for the early prediction of clinical outcomes of Non-Small Cell Lung Cancer (NSCLC) during radiotherapy or chemo-radiotherapy. A systematic review. *Eur J Nucl Med Mol Imaging.* (2017) 44:1915–27. doi: 10.1007/s00259-017-3762-9

11. Yamaguchi O, Kaira K, Hashimoto K, Mouri A, Shiono A, Miura Y, et al. Tumor metabolic volume by (18)F-FDG-PET as a prognostic predictor of first-line pembrolizumab for NSCLC patients with PD-L1 = 50. *Sci Rep.* (2020) 10:14990. doi: 10.1038/s41598-020-71735-y

12. Jadvar H, Alavi A, Gambhir SS. 18F-FDG uptake in lung, breast, and colon cancers: molecular biology correlates and disease characterization. *J Nucl Med.* (2009) 50:1820–7. doi: 10.2967/jnumed.108.054098

13. Hong JC, Boyer MJ, Spiegel DY, Williams CD, Tong BC, Shofer SL, et al. Increasing PET Use in Small Cell Lung Cancer: Survival Improvement and Stage Migration in the VA Central Cancer Registry. *J Natl Compr Canc Netw.* (2019) 17:127–39. doi: 10.6004/jnccn.2018.7090

14. Castello A, Rossi S, Lopci E. 18F-FDG PET/CT in restaging and evaluation of response to therapy in lung cancer: state of the art. *Curr Radiopharm.* (2020) 13:228–37. doi: 10.2174/1874471013666191230144821

15. Farsad M. FDG PET/CT in the Staging of Lung Cancer. *Curr Radiopharm.* (2020) 13:195–203. doi: 10.2174/1874471013666191223153755

16. Tamura M, Oda M, Matsumoto I, Waseda R, Watanabe G. Pattern and predictors of false positive lymph node involvement on positron emission tomography in patients with non-small cell lung cancer. *Thorac Cardiovasc Surg.* (2012) 60:105–10. doi: 10.1055/s-0031-1280068

17. Li S, Zheng Q, Ma Y, Wang Y, Feng Y, Zhao B, et al. Implications of false negative and false positive diagnosis in lymph node staging of NSCLC by means of ^{18}F-FDG PET/CT. *PLoS One.* (2013) 8:e78552. doi: 10.1371/journal.pone.0078552

18. Cuaron J, Dunphy M, Rimner A. Role of FDG-PET scans in staging, response assessment, and follow-up care for non-small cell lung cancer. *Front Oncol.* (2012) 2:208. doi: 10.3389/fonc.2012.00208

19. Telo S, Calderoni L, Vichi S, Zagni F, Castellucci P, Fanti S. Alternative and New Radiopharmaceutical Agents for Lung Cancer. *Curr Radiopharm.* (2020) 13:185–94. doi: 10.2174/1874471013666191223151402

20. Szyszko TA, Yip C, Szlosarek P, Goh V, Cook GJ. The role of new PET tracers for lung cancer. *Lung Cancer.* (2016) 94:7–14. doi: 10.1016/j.lungcan.2016.01.010

21. Martin B, Paesmans M, Mascaux C, Berghmans T, Lothaire P, Meert AP, et al. Ki-67 expression and patients survival in lung cancer: systematic review of the literature with meta-analysis. *Br J Cancer.* (2004) 91:2018–25. doi: 10.1038/sj.bjc.6602233

22. Vesselle H, Salskov A, Turcotte E, Wiens L, Schmidt R, Jordan CD, et al. Relationship between non-small cell lung cancer FDG uptake at PET, tumor histology, and Ki-67 proliferation index. *J Thorac Oncol.* (2008) 3:971–8. doi: 10.1097/JTO.0b013e31818307a7

23. Woo T, Okudela K, Yazawa T, Wada N, Ogawa N, Ishiwa N, et al. Prognostic value of KRAS mutations and Ki-67 expression in stage I lung adenocarcinomas. *Lung Cancer.* (2009) 65:355–62. doi: 10.1016/j.lungcan.2008.11.020

24. Duhaylongsod FG, Lowe VJ, Patz EF Jr., Vaughn AL, Coleman RE, Wolfe WG. Lung tumor growth correlates with glucose metabolism measured by fluoride-18 fluorodeoxyglucose positron emission tomography. *Ann Thorac Surg.* (1995) 60:1348–52. doi: 10.1016/0003-4975(95)00754-9

25. Vesselle H, Schmidt RA, Pugsley JM, Li M, Kohlmyer SG, Vallires E, et al. Lung cancer proliferation correlates with [F-18]fluorodeoxyglucose uptake by positron emission tomography. *Clin Cancer Res.* (2000) 6:3837–44.

26. Dooms C, van Baardwijk A, Verbeken E, van Suylen RJ, Stroobants S, De Ruysscher D, et al. Association between 18F-fluoro-2-deoxy-D-glucose uptake values and tumor vitality: prognostic value of positron emission tomography in early-stage non-small cell lung cancer. *J Thorac Oncol.* (2009) 4:822–8. doi: 10.1097/JTO.0b013e3181a97df7

27. Murakami S, Saito H, Sakuma Y, Mizutani Y, Ishikawa Y, Kondou T, et al. Correlation of 18F-fluorodeoxyglucose uptake on positron emission tomography with Ki-67 index and pathological invasive area in lung adenocarcinomas 30 mm or less in size. *Eur J Radiol.* (2010) 75:e62–6. doi: 10.1016/j.ejrad.2009.11.020

28. Chalkidou A, Landau DB, Odell EW, Cornelius VR, O'Doherty MJ, Marsden PK. Correlation between Ki-67 immunohistochemistry and 18F-fluorothymidine uptake in patients with cancer: A systematic review and meta-analysis. *Eur J Cancer.* (2012) 48:3499–513. doi: 10.1016/j.ejca.2012.05.001

29. Yang W, Zhang Y, Fu Z, Sun X, Mu D, Yu J. Imaging proliferation of ^{18}F-FLT PET/CT correlated with the expression of microvessel density of tumour tissue in non-small-cell lung cancer. *Eur J Nucl Med Mol Imaging.* (2012) 39:1289–96. doi: 10.1007/s00259-012-2126-8

30. Buck AK, Halter G, Schirrmeister H, Kotzerke J, Wurziger I, Glatting G, et al. Imaging proliferation in lung tumors with PET: 18F-FLT versus 18F-FDG. *J Nucl Med.* (2003) 44:1426–31.

31. Halter G, Buck AK, Schirrmeister H, Wurziger I, Liewald F, Glatting G, et al. [18F] 3-deoxy-3'-fluorothymidine positron emission tomography: alternative or diagnostic adjunct to 2-[18f]-fluoro-2-deoxy-D-glucose positron emission tomography in the workup of suspicious central focal lesions? *J Thorac Cardiovasc Surg.* (2004) 127:1093–9. doi: 10.1016/j.jtcvs.2003.09.003

32. Tian J, Yang X, Yu L, Chen P, Xin J, Ma L, et al. A multicenter clinical trial on the diagnostic value of dual-tracer PET/CT in pulmonary lesions using 3'-deoxy-3'-18F-fluorothymidine and 18F-FDG. *J Nucl Med.* (2008) 49:186–94. doi: 10.2967/jnumed.107.044966

33. Buck AK, Hetzel M, Schirrmeister H, Halter G, Möller P, Kratochwil C, et al. Clinical relevance of imaging proliferative activity in lung nodules. *Eur J Nucl Med Mol Imaging.* (2005) 32:525–33. doi: 10.1007/s00259-004-1706-7

34. Yang W, Zhang Y, Fu Z, Yu J, Sun X, Mu D, et al. Imaging of proliferation with 18F-FLT PET/CT versus 18F-FDG PET/CT in non-small-cell lung cancer. *Eur J Nucl Med Mol Imaging.* (2010) 37:1291–9. doi: 10.1007/s00259-010-1412-6

35. Everitt SJ, Ball DL, Hicks RJ, Callahan J, Plumridge N, Collins M, et al. Differential (18)F-FDG and (18)F-FLT Uptake on Serial PET/CT Imaging Before and During Definitive Chemoradiation for Non-Small Cell Lung Cancer. *J Nucl Med.* (2014) 55:1069–74. doi: 10.2967/jnumed.113.131631

36. Trigonis I, Koh PK, Taylor B, Tamal M, Ryder D, Earl M, et al. Early reduction in tumour [18F]fluorothymidine (FLT) uptake in patients with non-small cell lung cancer (NSCLC) treated with radiotherapy alone. *Eur J Nucl Med Mol Imaging.* (2014) 41:682–93. doi: 10.1007/s00259-013-2632-3

37. Kobe C, Scheffler M, Holstein A, Zander T, Nogova L, Lammertsma AA, et al. Predictive value of early and late residual 18F-fluorodeoxyglucose and 18F-fluorothymidine uptake using different SUV measurements in patients with non-small-cell lung cancer treated with erlotinib. *Eur J Nucl Med Mol Imaging.* (2012) 39:1117–27. doi: 10.1007/s00259-012-2118-8

38. Scheffler M, Zander T, Nogova L, Kobe C, Kahraman D, Dietlein M, et al. Prognostic impact of [18F]fluorothymidine and [18F]fluoro-D-glucose baseline uptakes in patients with lung cancer treated first-line with erlotinib. *PLoS One.* (2013) 8:e53081. doi: 10.1371/journal.pone.0053081

39. Chopra A. "Methyl-[(11)C]-4'-thiothymidine. *Molecular Imaging and Contrast Agent Database (MICAD).* Bethesda, MD: National Center for Biotechnology Information (2004).

40. Toyohara J, Elsinga PH, Ishiwata K, Sijbesma JW, Dierckx RA, van Waarde A. Evaluation of 4'-[methyl-11C]thiothymidine in a rodent tumor and inflammation model. *J Nucl Med.* (2012) 53:488–94. doi: 10.2967/jnumed.111.098426

41. Minamimoto R, Toyohara J, Seike A, Ito H, Endo H, Morooka M, et al. 4'-[Methyl-11C]-thiothymidine PET/CT for proliferation imaging in non-small cell lung cancer. *J Nucl Med.* (2012) 53:199–206. doi: 10.2967/jnumed.111.095539

42. Nishii R, Volgin AY, Mawlawi O, Mukhopadhyay U, Pal A, Bornmann W, et al. Evaluation of 2'-deoxy-2'-[18F]fluoro-5-methyl-1-beta-L: -arabinofuranosyluracil ([18F]-L: -FMAU) as a PET imaging agent for cellular proliferation: comparison with [18F]-D: -FMAU and [18F]FLT. *Eur J Nucl Med Mol Imaging.* (2008) 35:990–8. doi: 10.1007/s00259-007-0649-1

43. Sun H, Sloan A, Mangner TJ, Vaishampayan U, Muzik O, Collins JM, et al. Imaging DNA synthesis with [18F]FMAU and positron emission tomography in patients with cancer. *Eur J Nucl Med Mol Imaging.* (2005) 32:15–22. doi: 10.1007/s00259-004-1713-8

44. Shields AF. Positron emission tomography measurement of tumor metabolism and growth: its expanding role in oncology. *Mol Imaging Biol.* (2006) 8:141–50. doi: 10.1007/s11307-006-0039-2

45. Eiseman JL, Brown-Proctor C, Kinahan PE, Collins JM, Anderson LW, Joseph E, et al. Distribution of 1-(2-deoxy-2-fluoro-beta-D-arabinofuranosyl) uracil in mice bearing colorectal cancer xenografts: rationale for therapeutic use and as a positron emission tomography probe for thymidylate synthase. *Clin Cancer Res.* (2004) 10:6669–76. doi: 10.1158/1078-0432.ccr-03-0686

46. Calais J, Lussato D, Merlet P. Reply to "18F-Choline PET-CT in the management of lung cancer and mucinous tumors?". *J Thorac Oncol.* (2015) 10:e49–50. doi: 10.1097/jto.0000000000000527

47. Bauman G, Belhocine T, Kovacs M, Ward A, Beheshti M, Rachinsky I. 18F-fluorocholine for prostate cancer imaging: a systematic review of the literature. *Prostate Cancer Prostatic Dis.* (2012) 15:45–55. doi: 10.1038/pcan.2011.35

48. Kirienko M, Sollini M, Lopci E, Versari A, Chiti A. Applications of PET imaging with radiolabelled choline (11C/18F-choline). *Q J Nucl Med Mol Imaging.* (2015) 59:83–94.

49. Tian M, Zhang H, Oriuchi N, Higuchi T, Endo K. Comparison of 11C-choline PET and FDG PET for the differential diagnosis of malignant tumors. *Eur J Nucl Med Mol Imaging.* (2004) 31:1064–72. doi: 10.1007/s00259-004-1496-y

50. Huang Z, Rui J, Li X, Meng X, Liu Q. Use of ^{11}C-Choline positron emission tomography/computed tomography to investigate the mechanism of choline metabolism in lung cancer. *Mol Med Rep.* (2015) 11:3285–90. doi: 10.3892/mmr.2015.3200

51. Hara T, Kosaka N, Suzuki T, Kudo K, Niino H. Uptake rates of 18F-fluorodeoxyglucose and 11C-choline in lung cancer and pulmonary tuberculosis: a positron emission tomography study. *Chest.* (2003) 124:893–901. doi: 10.1378/chest.124.3.893

52. Vettore L, Westbrook RL, Tennant DA. New aspects of amino acid metabolism in cancer. *Br J Cancer.* (2020) 122:150–6. doi: 10.1038/s41416-019-0620-5

53. Kubota K, Yamada K, Fukada H, Endo S, Ito M, Abe Y, et al. Tumor detection with carbon-11-labelled amino acids. *Eur J Nucl Med.* (1984) 9:136–40. doi: 10.1007/bf00253516

54. Kubota K, Matsuzawa T, Ito M, Ito K, Fujiwara T, Abe Y, et al. Lung tumor imaging by positron emission tomography using C-11 L-methionine. *J Nucl Med.* (1985) 26:37–42.

55. Sasaki M, Kuwabara Y, Yoshida T, Nakagawa M, Koga H, Hayashi K, et al. Comparison of MET-PET and FDG-PET for differentiation between benign lesions and malignant tumors of the lung. *Ann Nucl Med.* (2001) 15:425–31. doi: 10.1007/bf02988346

56. Kanegae K, Nakano I, Kimura K, Kaji H, Kuge Y, Shiga T, et al. Comparison of MET-PET and FDG-PET for differentiation between benign lesions and lung cancer in pneumoconiosis. *Ann Nucl Med.* (2007) 21:331–7. doi: 10.1007/s12149-007-0035-x

57. Hsieh HJ, Lin SH, Lin KH, Lee CY, Chang CP, Wang SJ. The feasibility of 11C-methionine-PET in diagnosis of solitary lung nodules/masses when compared with 18F-FDG-PET. *Ann Nucl Med.* (2008) 22:533–8. doi: 10.1007/s12149-007-0142-8

58. Nariai T, Tanaka Y, Wakimoto H, Aoyagi M, Tamaki M, Ishiwata K, et al. Usefulness of L-[methyl-11C] methionine-positron emission tomography as a biological monitoring tool in the treatment of glioma. *J Neurosurg.* (2005) 103:498–507. doi: 10.3171/jns.2005.103.3.0498

59. Minamimoto R, Saginoya T, Kondo C, Tomura N, Ito K, Matsuo Y, et al. Differentiation of Brain Tumor Recurrence from Post-Radiotherapy Necrosis with 11C-Methionine PET: Visual Assessment versus Quantitative Assessment. *PLoS One.* (2015) 10:e0132515. doi: 10.1371/journal.pone.0132515

60. Kaira K, Oriuchi N, Shimizu K, Ishikita T, Higuchi T, Imai H, et al. Correlation of angiogenesis with 18F-FMT and 18F-FDG uptake in non-small cell lung cancer. *Cancer Sci.* (2009) 100:753–8. doi: 10.1111/j.1349-7006.2008.01077.x

61. Kaira K, Oriuchi N, Shimizu K, Tominaga H, Yanagitani N, Sunaga N, et al. 18F-FMT uptake seen within primary cancer on PET helps predict outcome of non-small cell lung cancer. *J Nucl Med.* (2009) 50:1770–6. doi: 10.2967/jnumed.109.066837

62. Wiriyasermkul P, Nagamori S, Tominaga H, Oriuchi N, Kaira K, Nakao H, et al. Transport of 3-fluoro-L-α-methyl-tyrosine by tumor-upregulated L-type amino acid transporter 1: a cause of the tumor uptake in PET. *J Nucl Med.* (2012) 53:1253–61. doi: 10.2967/jnumed.112.103069

63. Kaira K, Higuchi T, Sunaga N, Arisaka Y, Hisada T, Tominaga H, et al. Usefulness of 18F-α-Methyltyrosine PET for Therapeutic Monitoring of Patients with Advanced Lung Cancer. *Anticancer Res.* (2016) 36:6481–90. doi: 10.21873/anticanres.11247

64. Kumasaka S, Nakajima T, Arisaka Y, Tokue A, Achmad A, Fukushima Y, et al. Prognostic value of metabolic tumor volume of pretreatment (18)F-FAMT PET/CT in non-small cell lung Cancer. *BMC Med Imaging.* (2018) 18:46. doi: 10.1186/s12880-018-0292-2

65. Nishii R, Higashi T, Kagawa S, Kishibe Y, Takahashi M, Yamauchi H, et al. Diagnostic usefulness of an amino acid tracer, α-[N-methyl-(11)C]-methylaminoisobutyric acid ((11)C-MeAIB), in the PET diagnosis of chest malignancies. *Ann Nucl Med.* (2013) 27:808–21. doi: 10.1007/s12149-013-0750-4

66. Smolarz K, Krause BJ, Graner FP, Wagner FM, Hultsch C, Bacher-Stier C, et al. (S)-4-(3-18F-fluoropropyl)-L-glutamic acid: an 18F-labeled tumor-specific probe for PET/CT imaging–dosimetry. *J Nucl Med.* (2013) 54:861–6. doi: 10.2967/jnumed.112.112581

67. Jager PL, Vaalburg W, Pruim J, de Vries EG, Langen KJ, Piers DA. Radiolabeled amino acids: basic aspects and clinical applications in oncology. *J Nucl Med.* (2001) 42:432–45.

68. Laverman P, Boerman OC, Corstens FH, Oyen WJ. Fluorinated amino acids for tumour imaging with positron emission tomography. *Eur J Nucl Med Mol Imaging.* (2002) 29:681–90. doi: 10.1007/s00259-001-0716-y

69. Huang C, McConathy J. Radiolabeled amino acids for oncologic imaging. *J Nucl Med.* (2013) 54:1007–10. doi: 10.2967/jnumed.112.113100

70. Qi Y, Liu X, Li J, Yao H, Yuan S. Fluorine-18 labeled amino acids for tumor PET/CT imaging. *Oncotarget.* (2017) 8:60581–8. doi: 10.18632/oncotarget.19943

71. Law I, Albert NL, Arbizu J, Boellaard R, Drzezga A, Galldiks N, et al. Joint EANM/EANO/RANO practice guidelines/SNMMI procedure standards for imaging of gliomas using PET with radiolabelled amino acids and [(18)F]FDG: version 1.0. *Eur J Nucl Med Mol Imaging.* (2019) 46:540–57. doi: 10.1007/s00259-018-4207-9

72. Kurihara H, Honda N, Kono Y, Arai Y. Radiolabelled agents for PET imaging of tumor hypoxia. *Curr Med Chem.* (2012) 19:3282–9. doi: 10.2174/092986712801215964

73. Yip C, Blower PJ, Goh V, Landau DB, Cook GJ. Molecular imaging of hypoxia in non-small-cell lung cancer. *Eur J Nucl Med Mol Imaging.* (2015) 42:956–76. doi: 10.1007/s00259-015-3009-6

74. Jerabek PA, Patrick TB, Kilbourn MR, Dischino DD, Welch MJ. Synthesis and biodistribution of 18F-labeled fluoronitroimidazoles: potential in vivo markers of hypoxic tissue. *Int J Rad Appl Instrum A.* (1986) 37:599–605. doi: 10.1016/0883-2889(86)90079-1

75. Kubota K, Tada M, Yamada S, Hori K, Saito S, Iwata R, et al. Comparison of the distribution of fluorine-18 fluoromisonidazole, deoxyglucose and methionine in tumour tissue. *Eur J Nucl Med.* (1999) 26:750–7. doi: 10.1007/s002590050446

76. Gagel B, Reinartz P, Dimartino E, Zimny M, Pinkawa M, Maneschi P, et al. pO(2) Polarography versus positron emission tomography ([(18)F] fluoromisonidazole, [(18)F]-2-fluoro-2'-deoxyglucose). An appraisal of radiotherapeutically relevant hypoxia. *Strahlenther Onkol.* (2004) 180:616–22. doi: 10.1007/s00066-004-1229-y

77. Lawrentschuk N, Poon AM, Foo SS, Putra LG, Murone C, Davis ID, et al. Assessing regional hypoxia in human renal tumours using 18F-fluoromisonidazole positron emission tomography. *BJU Int.* (2005) 96:540–6. doi: 10.1111/j.1464-410X.2005.05681.x

78. Zimny M, Gagel B, DiMartino E, Hamacher K, Coenen HH, Westhofen M, et al. FDG–a marker of tumour hypoxia? A comparison with [18F]fluoromisonidazole and pO2-polarography in metastatic head and neck cancer. *Eur J Nucl Med Mol Imaging.* (2006) 33:1426–31. doi: 10.1007/s00259-006-0175-6

79. Gagel B, Piroth M, Pinkawa M, Reinartz P, Zimny M, Kaiser HJ, et al. pO polarography, contrast enhanced color duplex sonography (CDS), [18F] fluoromisonidazole and [18F] fluorodeoxyglucose positron emission tomography: validated methods for the evaluation of therapy-relevant tumor oxygenation or only bricks in the puzzle of tumor hypoxia? *BMC Cancer.* (2007) 7:113. doi: 10.1186/1471-2407-7-113

80. Bentzen L, Keiding S, Horsman MR, Falborg L, Hansen SB, Overgaard J. Feasibility of detecting hypoxia in experimental mouse tumours with 18F-fluorinated tracers and positron emission tomography–a study evaluating [18F]Fluoro-2-deoxy-D-glucose. *Acta Oncol.* (2000) 39:629–37. doi: 10.1080/028418600750013320

81. Wyss MT, Honer M, Schubiger PA, Ametamey SM. NanoPET imaging of [(18)F]fluoromisonidazole uptake in experimental mouse tumours. *Eur J Nucl Med Mol Imaging.* (2006) 33:311–8. doi: 10.1007/s00259-005-1951-4

82. Oswald J, Treite F, Haase C, Kampfrath T, Mäding P, Schwenzer B, et al. Experimental hypoxia is a potent stimulus for radiotracer uptake in vitro: comparison of different tumor cells and primary endothelial cells. *Cancer Lett.* (2007) 254:102–10. doi: 10.1016/j.canlet.2007.02.016

83. Hicks RJ, Rischin D, Fisher R, Binns D, Scott AM, Peters LJ. Utility of FMISO PET in advanced head and neck cancer treated with chemoradiation incorporating a hypoxia-targeting chemotherapy agent. *Eur J Nucl Med Mol Imaging.* (2005) 32:1384–91. doi: 10.1007/s00259-005-1880-2

84. Rajendran JG, Schwartz DL, O'Sullivan J, Peterson LM, Ng P, Scharnhorst J, et al. Tumor hypoxia imaging with [F-18] fluoromisonidazole positron emission tomography in head and neck cancer. *Clin Cancer Res.* (2006) 12:5435–41. doi: 10.1158/1078-0432.Ccr-05-1773

85. Rischin D, Hicks RJ, Fisher R, Binns D, Corry J, Porceddu S, et al. Prognostic significance of [18F]-misonidazole positron emission tomography-detected tumor hypoxia in patients with advanced head and neck cancer randomly assigned to chemoradiation with or without tirapazamine: a substudy of Trans-Tasman Radiation Oncology Group Study 98.02. *J Clin Oncol.* (2006) 24:2098–104. doi: 10.1200/jco.2005.05.2878

86. Gagel B, Reinartz P, Demirel C, Kaiser HJ, Zimny M, Piroth M, et al. [18F] fluoromisonidazole and [18F] fluorodeoxyglucose positron emission tomography in response evaluation after chemo-/radiotherapy of non-small-cell lung cancer: a feasibility study. *BMC Cancer.* (2006) 6:51. doi: 10.1186/1471-2407-6-51

87. Ballinger JR. Imaging hypoxia in tumors. *Semin Nucl Med* (2001) 31:321–9. doi: 10.1053/snuc.2001.26191

88. Yang DJ, Wallace S, Cherif A, Li C, Gretzer MB, Kim EE, et al. Development of F-18-labeled fluoroerythronitroimidazole as a PET agent for imaging tumor hypoxia. *Radiology.* (1995) 194:795–800. doi: 10.1148/radiology.194.3.7862981

89. Li L, Hu M, Zhu H, Zhao W, Yang G, Yu J. Comparison of 18F-Fluoroerythronitroimidazole and 18F-fluorodeoxyglucose positron emission tomography and prognostic value in locally advanced non-small-cell lung cancer. *Clin Lung Cancer.* (2010) 11:335–40. doi: 10.3816/CLC.2010.n.042

90. Hu M, Xing L, Mu D, Yang W, Yang G, Kong L, et al. Hypoxia imaging with 18F-fluoroerythronitroimidazole integrated PET/CT and immunohistochemical studies in non-small cell lung cancer. *Clin Nucl Med.* (2013) 38:591–6. doi: 10.1097/RLU.0b013e318279fd3d

91. Lehtiö K, Eskola O, Viljanen T, Oikonen V, Grönroos T, Sillanmäki L, et al. Imaging perfusion and hypoxia with PET to predict radiotherapy response in head-and-neck cancer. *Int J Radiat Oncol Biol Phys.* (2004) 59:971–82. doi: 10.1016/j.ijrobp.2003.12.014

92. Dubois LJ, Lieuwes NG, Janssen MH, Peeters WJ, Windhorst AD, Walsh JC, et al. Preclinical evaluation and validation of [18F]HX4, a promising hypoxia marker for PET imaging. *Proc Natl Acad Sci USA.* (2011) 108:14620–5. doi: 10.1073/pnas.1102526108

93. Chen L, Zhang Z, Kolb HC, Walsh JC, Zhang J, Guan Y. ^{18}F-HX4 hypoxia imaging with PET/CT in head and neck cancer: a comparison with ^{18}F-FMISO. *Nucl Med Commun.* (2012) 33:1096–102. doi: 10.1097/MNM.0b013e3283571016

94. Busk M, Horsman MR, Jakobsen S, Bussink J, van der Kogel A, Overgaard J. Cellular uptake of PET tracers of glucose metabolism and hypoxia and their linkage. *Eur J Nucl Med Mol Imaging.* (2008) 35:2294–303. doi: 10.1007/s00259-008-0888-9

95. Piert M, Machulla HJ, Picchio M, Reischl G, Ziegler S, Kumar P, et al. Hypoxia-specific tumor imaging with 18F-fluoroazomycin arabinoside. *J Nucl Med.* (2005) 46:106–13.

96. Busk M, Horsman MR, Jakobsen S, Keiding S, van der Kogel AJ, Bussink J, et al. Imaging hypoxia in xenografted and murine tumors with 18F-fluoroazomycin arabinoside: a comparative study involving microPET, autoradiography, PO2-polarography, and fluorescence microscopy. *Int J Radiat Oncol Biol Phys.* (2008) 70:1202–12. doi: 10.1016/j.ijrobp.2007.11.034

97. Saga T, Inubushi M, Koizumi M, Yoshikawa K, Zhang MR, Tanimoto K, et al. Prognostic value of (18) F-fluoroazomycin arabinoside PET/CT in patients with advanced non-small-cell lung cancer. *Cancer Sci.* (2015) 106:1554–60. doi: 10.1111/cas.12771

98. Di Perri D, Lee JA, Bol A, Hanin FX, Janssens G, Labar D, et al. Correlation analysis of [(18)F]fluorodeoxyglucose and [(18)F]fluoroazomycin arabinoside uptake distributions in lung tumours during radiation therapy. *Acta Oncol.* (2017) 56:1181–8. doi: 10.1080/0284186x.2017.1329594

99. Patt M, Sorger D, Scheunemann M, Stöcklin G. Adduct of 2-[18F]FDG and 2-nitroimidazole as a putative radiotracer for the detection of hypoxia with PET: synthesis, in vitro- and in vivo-characterization. *Appl Radiat Isot.* (2002) 57:705–12. doi: 10.1016/s0969-8043(02)00186-0

100. Yamamoto F, Aoki M, Furusawa Y, Ando K, Kuwabara Y, Masuda K, et al. Synthesis and evaluation of 4-bromo-1-(3-[18F]fluoropropyl)-2-nitroimidazole with a low energy LUMO orbital designed as brain hypoxia-targeting imaging agent. *Biol Pharm Bull.* (2002) 25:616–21. doi: 10.1248/bpb.25.616

101. Mahy P, De Bast M, Gillart J, Labar D, Grégoire V. Detection of tumour hypoxia: comparison between EF5 adducts and [18F]EF3 uptake on an individual mouse tumour basis. *Eur J Nucl Med Mol Imaging.* (2006) 33:553–6. doi: 10.1007/s00259-005-0049-3

102. Riedl CC, Brader P, Zanzonico P, Reid V, Woo Y, Wen B, et al. Tumor hypoxia imaging in orthotopic liver tumors and peritoneal metastasis: a comparative study featuring dynamic 18F-MISO and 124I-IAZG PET in the same study cohort. *Eur J Nucl Med Mol Imaging.* (2008) 35:39–46. doi: 10.1007/s00259-007-0522-2

103. Riedl CC, Brader P, Zanzonico PB, Chun YS, Woo Y, Singh P, et al. Imaging hypoxia in orthotopic rat liver tumors with iodine 124-labeled iodoazomycin galactopyranoside PET. *Radiology.* (2008) 248:561–70. doi: 10.1148/radiol.2482071421

104. O'Donoghue JA, Guillem JG, Schöder H, Lee NY, Divgi CR, Ruby JA, et al. Pilot study of PET imaging of 124I-iodoazomycin galactopyranoside (IAZGP), a putative hypoxia imaging agent, in patients with colorectal cancer and head and neck cancer. *EJNMMI Res.* (2013) 3:42. doi: 10.1186/2191-219x-3-42

105. Fujibayashi Y, Taniuchi H, Yonekura Y, Ohtani H, Konishi J, Yokoyama A. Copper-62-ATSM: a new hypoxia imaging agent with high membrane permeability and low redox potential. *J Nucl Med.* (1997) 38:1155–60.

106. Dearling JL, Lewis JS, Mullen GE, Rae MT, Zweit J, Blower PJ. Design of hypoxia-targeting radiopharmaceuticals: selective uptake of copper-64 complexes in hypoxic cells in vitro. *Eur J Nucl Med.* (1998) 25:788–92. doi: 10.1007/s002590050283

107. Lewis JS, McCarthy DW, McCarthy TJ, Fujibayashi Y, Welch MJ. Evaluation of 64Cu-ATSM in vitro and in vivo in a hypoxic tumor model. *J Nucl Med.* (1999) 40:177–83.

108. Lewis JS, Sharp TL, Laforest R, Fujibayashi Y, Welch MJ. Tumor uptake of copper-diacetyl-bis(N(4)-methylthiosemicarbazone): effect of changes in tissue oxygenation. *J Nucl Med.* (2001) 42:655–61.

109. O'Donoghue JA, Zanzonico P, Pugachev A, Wen B, Smith-Jones P, Cai S, et al. Assessment of regional tumor hypoxia using 18F-fluoromisonidazole and 64Cu(II)-diacetyl-bis(N4-methylthiosemicarbazone) positron emission tomography: Comparative study featuring microPET imaging, Po2 probe measurement, autoradiography, and fluorescent microscopy in the R3327-AT and FaDu rat tumor models. *Int J Radiat Oncol Biol Phys.* (2005) 61:1493–502. doi: 10.1016/j.ijrobp.2004.12.057

110. Tanaka T, Furukawa T, Fujieda S, Kasamatsu S, Yonekura Y, Fujibayashi Y. Double-tracer autoradiography with Cu-ATSM/FDG and immunohistochemical interpretation in four different mouse implanted tumor models. *Nucl Med Biol.* (2006) 33:743–50. doi: 10.1016/j.nucmedbio.2006.05.005

111. Oh M, Tanaka T, Kobayashi M, Furukawa T, Mori T, Kudo T, et al. Radiocopper-labeled Cu-ATSM: an indicator of quiescent but clonogenic cells under mild hypoxia in a Lewis lung carcinoma model. *Nucl Med Biol.* (2009) 36:419–26. doi: 10.1016/j.nucmedbio.2009.01.016

112. Chao KS, Bosch WR, Mutic S, Lewis JS, Dehdashti F, Mintun MA, et al. A novel approach to overcome hypoxic tumor resistance: Cu-ATSM-guided intensity-modulated radiation therapy. *Int J Radiat Oncol Biol Phys.* (2001) 49:1171–82. doi: 10.1016/s0360-3016(00)01433-4

113. Dehdashti F, Mintun MA, Lewis JS, Bradley J, Govindan R, Laforest R, et al. In vivo assessment of tumor hypoxia in lung cancer with 60Cu-ATSM. *Eur J Nucl Med Mol Imaging.* (2003) 30:844–50. doi: 10.1007/s00259-003-1130-4

114. Dehdashti F, Grigsby PW, Lewis JS, Laforest R, Siegel BA, Welch MJ. Assessing tumor hypoxia in cervical cancer by PET with 60Cu-labeled diacetyl-bis(N4-methylthiosemicarbazone). *J Nucl Med.* (2008) 49:201–5. doi: 10.2967/jnumed.107.048520

115. Zhang T, Das SK, Fels DR, Hansen KS, Wong TZ, Dewhirst MW, et al. PET with 62Cu-ATSM and 62Cu-PTSM is a useful imaging tool for hypoxia and perfusion in pulmonary lesions. *AJR Am J Roentgenol.* (2013) 201:W698–706. doi: 10.2214/ajr.12.9698

116. Kinoshita T, Fujii H, Hayashi Y, Kamiyama I, Ohtsuka T, Asamura H. Prognostic significance of hypoxic PET using (18)F-FAZA and (62)Cu-ATSM in

non-small-cell lung cancer. *Lung Cancer.* (2016) 91:56–66. doi: 10.1016/j.lungcan.2015.11.020

117. Lopci E, Grassi I, Rubello D, Colletti PM, Cambioli S, Gamboni A, et al. Prognostic Evaluation of Disease Outcome in Solid Tumors Investigated With 64Cu-ATSM PET/CT. *Clin Nucl Med.* (2016) 41:e87–92. doi: 10.1097/rlu.0000000000001017

118. Folkman J. Angiogenesis in cancer, vascular, rheumatoid and other disease. *Nat Med* (1995) 1:27–31. doi: 10.1038/nm0195-27

119. Sipkins DA, Cheresh DA, Kazemi MR, Nevin LM, Bednarski MD, Li KC. Detection of tumor angiogenesis in vivo by alphaVbeta3-targeted magnetic resonance imaging. *Nat Med.* (1998) 4:623–6. doi: 10.1038/nm0598-623

120. Bruce D, Tan PH. Vascular endothelial growth factor receptors and the therapeutic targeting of angiogenesis in cancer: where do we go from here? *Cell Commun Adhes.* (2011) 18:85–103. doi: 10.3109/15419061.2011.619673

121. Stacy MR, Maxfield MW, Sinusas AJ. Targeted molecular imaging of angiogenesis in PET and SPECT: a review. *Yale J Biol Med.* (2012) 85:75–86.

122. Simons M. Angiogenesis: where do we stand now? *Circulation.* (2005) 111:1556–66. doi: 10.1161/01.Cir.0000159345.00591.8f

123. Carmeliet P, Jain RK. Molecular mechanisms and clinical applications of angiogenesis. *Nature.* (2011) 473:298–307. doi: 10.1038/nature10144

124. Schwartz MA, Schaller MD, Ginsberg MH. Integrins: emerging paradigms of signal transduction. *Annu Rev Cell Dev Biol.* (1995) 11:549–99. doi: 10.1146/annurev.cb.11.110195.003001

125. Meoli DF, Sadeghi MM, Krassilnikova S, Bourke BN, Giordano FJ, Dione DP, et al. Noninvasive imaging of myocardial angiogenesis following experimental myocardial infarction. *J Clin Invest.* (2004) 113:1684–91. doi: 10.1172/jci20352

126. Hua J, Dobrucki LW, Sadeghi MM, Zhang J, Bourke BN, Cavaliere P, et al. Noninvasive imaging of angiogenesis with a 99mTc-labeled peptide targeted at alphavbeta3 integrin after murine hindlimb ischemia. *Circulation.* (2005) 111:3255–60. doi: 10.1161/circulationaha.104.485029

127. Dobrucki LW, Dione DP, Kalinowski L, Dione D, Mendizabal M, Yu J, et al. Serial noninvasive targeted imaging of peripheral angiogenesis: validation and application of a semiautomated quantitative approach. *J Nucl Med.* (2009) 50:1356–63. doi: 10.2967/jnumed.108.060822

128. Liang W, Wu X, Hong S, Zhang Y, Kang S, Fang W, et al. Multi-targeted antiangiogenic tyrosine kinase inhibitors in advanced non-small cell lung cancer: meta-analyses of 20 randomized controlled trials and subgroup analyses. *PLoS One.* (2014) 9:e109757. doi: 10.1371/journal.pone.0109757

129. Luo H, England CG, Graves SA, Sun H, Liu G, Nickles RJ, et al. PET Imaging of VEGFR-2 Expression in Lung Cancer with 64Cu-Labeled Ramucirumab. *J Nucl Med.* (2016) 57:285–90. doi: 10.2967/jnumed.115.166462

130. Nayak TK, Garmestani K, Baidoo KE, Milenic DE, Brechbiel MW. PET imaging of tumor angiogenesis in mice with VEGF-A-targeted (86)Y-CHX-A?-DTPA-bevacizumab. *Int J Cancer.* (2011) 128:920–6. doi: 10.1002/ijc.25409

131. Bahce I, Huisman MC, Verwer EE, Ooijevaar R, Boutkourt F, Vugts DJ, et al. Pilot study of (89)Zr-bevacizumab positron emission tomography in patients with advanced non-small cell lung cancer. *EJNMMI Res.* (2014) 4:35. doi: 10.1186/s13550-014-0035-5

132. Chen X, Sievers E, Hou Y, Park R, Tohme M, Bart R, et al. Integrin alpha v beta 3-targeted imaging of lung cancer. *Neoplasia.* (2005) 7:271–9. doi: 10.1593/neo.04538

133. Haubner R. Alphavbeta3-integrin imaging: a new approach to characterise angiogenesis? *Eur J Nucl Med Mol Imaging.* (2006) 33(Suppl 1):54–63. doi: 10.1007/s00259-006-0136-0

134. Beer AJ, Lorenzen S, Metz S, Herrmann K, Watzlowik P, Wester HJ, et al. Comparison of integrin alphaVbeta3 expression and glucose metabolism in primary and metastatic lesions in cancer patients: a PET study using 18F-galacto-RGD and 18F-FDG. *J Nucl Med.* (2008) 49:22–9. doi: 10.2967/jnumed.107.045864

135. Zheng K, Liang N, Zhang J, Lang L, Zhang W, Li S, et al. 68Ga-NOTA-PRGD2 PET/CT for Integrin Imaging in Patients with Lung Cancer. *J Nucl Med.* (2015) 56:1823–7. doi: 10.2967/jnumed.115.160648

136. Kang F, Wang S, Tian F, Zhao M, Zhang M, Wang Z, et al. Comparing the Diagnostic Potential of 68Ga-Alfatide II and 18F-FDG in Differentiating Between Non-Small Cell Lung Cancer and Tuberculosis. *J Nucl Med.* (2016) 57:672–7. doi: 10.2967/jnumed.115.167924

137. Lang L, Li W, Guo N, Ma Y, Zhu L, Kiesewetter DO, et al. Comparison study of [18F]FAl-NOTA-PRGD2, [18F]FPPRGD2, and [68Ga]Ga-NOTA-PRGD2 for PET imaging of U87MG tumors in mice. *Bioconjug Chem.* (2011) 22:2415–22. doi: 10.1021/bc200197h

138. Wan W, Guo N, Pan D, Yu C, Weng Y, Luo S, et al. First experience of 18F-alfatide in lung cancer patients using a new lyophilized kit for rapid radiofluorination. *J Nucl Med.* (2013) 54:691–8. doi: 10.2967/jnumed.112.113563

139. Luan X, Huang Y, Gao S, Sun X, Wang S, Ma L, et al. (18)F-alfatide PET/CT may predict short-term outcome of concurrent chemoradiotherapy in patients with advanced non-small cell lung cancer. *Eur J Nucl Med Mol Imaging.* (2016) 43:2336–42. doi: 10.1007/s00259-016-3505-3

140. Hendifar AE, Marchevsky AM, Tuli R. Neuroendocrine tumors of the lung: current challenges and advances in the diagnosis and management of well-differentiated disease. *J Thorac Oncol.* (2017) 12:425–36. doi: 10.1016/j.jtho.2016.11.2222

141. Wolin EM. Advances in the diagnosis and management of well-differentiated and intermediate-differentiated neuroendocrine tumors of the lung. *Chest.* (2017) 151:1141–6. doi: 10.1016/j.chest.2016.06.018

142. Ambrosini V, Tomassetti P, Castellucci P, Campana D, Montini G, Rubello D, et al. Comparison between 68Ga-DOTA-NOC and 18F-DOPA PET for the detection of gastro-entero-pancreatic and lung neuro-endocrine tumours. *Eur J Nucl Med Mol Imaging.* (2008) 35:1431–8. doi: 10.1007/s00259-008-0769-2

143. Liu Y. Lung Neoplasms with Low F18-Fluorodeoxyglucose Avidity. *PET Clin.* (2018) 13:11–8. doi: 10.1016/j.cpet.2017.08.002

144. Cheng G. Non-Small-Cell Lung Cancer PET Imaging Beyond F18 Fluorodeoxyglucose. *PET Clin.* (2018) 13:73–81. doi: 10.1016/j.cpet.2017.09.006

145. Deppen SA, Blume J, Bobbey AJ, Shah C, Graham MM, Lee P, et al. 68Ga-DOTATATE Compared with 111In-DTPA-Octreotide and Conventional Imaging for Pulmonary and Gastroenteropancreatic Neuroendocrine Tumors: A Systematic Review and Meta-Analysis. *J Nucl Med.* (2016) 57:872–8. doi: 10.2967/jnumed.115.165803

146. Venkitaraman B, Karunanithi S, Kumar A, Khilnani GC, Kumar R. Role of 68Ga-DOTATOC PET/CT in initial evaluation of patients with suspected bronchopulmonary carcinoid. *Eur J Nucl Med Mol Imaging.* (2014) 41:856–64. doi: 10.1007/s00259-013-2659-5

147. Walker R, Deppen S, Smith G, Shi C, Lehman J, Clanton J, et al. 68Ga-DOTATATE PET/CT imaging of indeterminate pulmonary nodules and lung cancer. *PLoS One.* (2017) 12:e0171301. doi: 10.1371/journal.pone.0171301

148. Kayani I, Conry BG, Groves AM, Win T, Dickson J, Caplin M, et al. A comparison of 68Ga-DOTATATE and 18F-FDG PET/CT in pulmonary neuroendocrine tumors. *J Nucl Med.* (2009) 50:1927–32. doi: 10.2967/jnumed.109.066639

149. Kumar A, Jindal T, Dutta R, Kumar R. Functional imaging in differentiating bronchial masses: an initial experience with a combination of (18)F-FDG PET-CT scan and (68)Ga DOTA-TOC PET-CT scan. *Ann Nucl Med.* (2009) 23:745–51. doi: 10.1007/s12149-009-0302-0

150. Jindal T, Kumar A, Venkitaraman B, Meena M, Kumar R, Malhotra A, et al. Evaluation of the role of [18F]FDG-PET/CT and [68Ga]DOTATOC-PET/CT in differentiating typical and atypical pulmonary carcinoids. *Cancer Imaging.* (2011) 11:70–5. doi: 10.1102/1470-7330.2011.0010

151. Zheng Y, Zhu Z. A proof-of-concept study of &Itsup&gt68&It/sup&gtGa-NOTA-3P-TATE-RGD PET/CT for dual-target imaging of somatostatin receptor and integrin α&Itsub&gtv&It/sub&gtβ&Itsub&gt3&It/sub&gt to detect lung cancer in a single scan. *J Nucl Med.* (2018) 59(suppl 1):1141.

152. Zheng Y, Wang H, Tan H, Cui X, Yao S, Zang J, et al. Evaluation of Lung Cancer and Neuroendocrine Neoplasm in a Single Scan by Targeting Both Somatostatin Receptor and Integrin αvβ3. *Clin Nucl Med.* (2019) 44:687–94. doi: 10.1097/rlu.0000000000002680

153. Rylova SN, Stoykow C, Del Pozzo L, Abiraj K, Tamma ML, Kiefer Y, et al. The somatostatin receptor 2 antagonist 64Cu-NODAGA-JR11 outperforms 64Cu-DOTA-TATE in a mouse xenograft model. *PLoS One.* (2018) 13:e0195802. doi: 10.1371/journal.pone.0195802

154. Xie Q, Liu T, Ding J, Zhou N, Meng X, Zhu H, et al. Synthesis, preclinical evaluation, and a pilot clinical imaging study of [(18)F]AlF-NOTA-JR11 for neuroendocrine neoplasms compared with [(68)Ga]Ga-DOTA-TATE. *Eur J Nucl Med Mol Imaging.* (2021) 48:3129–40. doi: 10.1007/s00259-021-05249-8

155. Zhu W, Cheng Y, Wang X, Yao S, Bai C, Zhao H, et al. Head-to-Head Comparison of (68)Ga-DOTA-JR11 and (68)Ga-DOTATATE PET/CT in Patients with Metastatic, Well-Differentiated Neuroendocrine Tumors: A Prospective Study. *J Nucl Med.* (2020) 61:897–903. doi: 10.2967/jnumed.119.235093

156. Garnett ES, Firnau G, Nahmias C. Dopamine visualized in the basal ganglia of living man. *Nature.* (1983) 305:137–8. doi: 10.1038/305137a0

157. Heiss WD, Wienhard K, Wagner R, Lanfermann H, Thiel A, Herholz K, et al. F-Dopa as an amino acid tracer to detect brain tumors. *J Nucl Med.* (1996) 37:1180–2.

158. Becherer A, Szabó M, Karanikas G, Wunderbaldinger P, Angelberger P, Raderer M, et al. Imaging of advanced neuroendocrine tumors with (18)F-FDOPA PET. *J Nucl Med.* (2004) 45:1161–7.

159. Koopmans KP, de Vries EG, Kema IP, Elsinga PH, Neels OC, Sluiter WJ, et al. Staging of carcinoid tumours with 18F-DOPA PET: a prospective, diagnostic accuracy study. *Lancet Oncol.* (2006) 7:728–34. doi: 10.1016/s1470-2045(06)70801-4

160. Maffione AM, Grassetto G, Rampin L, Chondrogiannis S, Marzola MC, Ambrosini V, et al. Molecular imaging of pulmonary nodules. *AJR Am J Roentgenol.* (2014) 202:W217–23. doi: 10.2214/ajr.13.11733

161. Caroli P, Nanni C, Rubello D, Alavi A, Fanti S. Non-FDG PET in the practice of oncology. *Indian J Cancer.* (2010) 47:120–5. doi: 10.4103/0019-509x.62998

162. Haug A, Auernhammer CJ, Wängler B, Tiling R, Schmidt G, Göke B, et al. Intraindividual comparison of 68Ga-DOTA-TATE and 18F-DOPA PET in patients with well-differentiated metastatic neuroendocrine tumours. *Eur J Nucl Med Mol Imaging.* (2009) 36:765–70. doi: 10.1007/s00259-008-1030-8

163. Maulik G, Kijima T, Salgia R. Role of receptor tyrosine kinases in lung cancer. *Methods Mol Med.* (2003) 74:113–25. doi: 10.1385/1-59259-323-2:113

164. Pisick E, Jagadeesh S, Salgia R. Receptor tyrosine kinases and inhibitors in lung cancer. *ScientificWorldJournal.* (2004) 4:589–604. doi: 10.1100/tsw.2004.117

165. Zheng D, Wang R, Ye T, Yu S, Hu H, Shen X, et al. MET exon 14 skipping defines a unique molecular class of non-small cell lung cancer. *Oncotarget.* (2016) 7:41691–702. doi: 10.18632/oncotarget.9541

166. Perk LR, Visser GW, Vosjan MJ, Stigter-van Walsum M, Tijink BM, Leemans CR, et al. (89)Zr as a PET surrogate radioisotope for scouting biodistribution of the therapeutic radiometals (90)Y and (177)Lu in tumor-bearing nude mice after coupling to the internalizing antibody cetuximab. *J Nucl Med.* (2005) 46:1898–906.

167. Cai W, Chen K, He L, Cao Q, Koong A, Chen X. Quantitative PET of EGFR expression in xenograft-bearing mice using 64Cu-labeled cetuximab, a chimeric anti-EGFR monoclonal antibody. *Eur J Nucl Med Mol Imaging.* (2007) 34:850–8. doi: 10.1007/s00259-006-0361-6

168. Niu G, Li Z, Xie J, Le QT, Chen X. PET of EGFR antibody distribution in head and neck squamous cell carcinoma models. *J Nucl Med.* (2009) 50:1116–23. doi: 10.2967/jnumed.109.061820

169. Bhattacharyya S, Kurdziel K, Wei L, Riffle L, Kaur G, Hill GC, et al. Zirconium-89 labeled panitumumab: a potential immuno-PET probe for HER1-expressing carcinomas. *Nucl Med Biol.* (2013) 40:451–7. doi: 10.1016/j.nucmedbio.2013.01.007

170. van Loon J, Even AJG, Aerts H, Öllers M, Hoebers F, van Elmpt W, et al. PET imaging of zirconium-89 labelled cetuximab: A phase I trial in patients with head and neck and lung cancer. *Radiother Oncol.* (2017) 122:267–73. doi: 10.1016/j.radonc.2016.11.020

171. Menke-van der Houven van Oordt CW, Gootjes EC, Huisman MC, Vugts DJ, Roth C, Luik AM, et al. 89Zr-cetuximab PET imaging in patients with advanced colorectal cancer. *Oncotarget.* (2015) 6:30384–93. doi: 10.18632/oncotarget.4672

172. Wang H, Yu J, Yang G, Song X, Sun X, Zhao S, et al. Assessment of 11C-labeled-4-N-(3-bromoanilino)-6,7-dimethoxyquinazoline as a positron emission tomography agent to monitor epidermal growth factor receptor expression. *Cancer Sci.* (2007) 98:1413–6. doi: 10.1111/j.1349-7006.2007.00562.x

173. Dai D, Li XF, Wang J, Liu JJ, Zhu YJ, Zhang Y, et al. Predictive efficacy of (11)C-PD153035 PET imaging for EGFR-tyrosine kinase inhibitor sensitivity in non-small cell lung cancer patients. *Int J Cancer.* (2016) 138:1003–12. doi: 10.1002/ijc.29832

174. Meng X, Loo BW Jr., Ma L, Murphy JD, Sun X, Yu J. Molecular imaging with 11C-PD153035 PET/CT predicts survival in non-small cell lung cancer treated with EGFR-TKI: a pilot study. *J Nucl Med.* (2011) 52:1573–9. doi: 10.2967/jnumed.111.092874

175. Memon AA, Jakobsen S, Dagnaes-Hansen F, Sorensen BS, Keiding S, Nexo E. Positron emission tomography (PET) imaging with [11C]-labeled erlotinib: a micro-PET study on mice with lung tumor xenografts. *Cancer Res.* (2009) 69:873–8. doi: 10.1158/0008-5472.Can-08-3118

176. Memon AA, Weber B, Winterdahl M, Jakobsen S, Meldgaard P, Madsen HH, et al. PET imaging of patients with non-small cell lung cancer employing an EGF receptor targeting drug as tracer. *Br J Cancer.* (2011) 105:1850–5. doi: 10.1038/bjc.2011.493

177. Weber B, Winterdahl M, Memon A, Sorensen BS, Keiding S, Sorensen L, et al. Erlotinib accumulation in brain metastases from non-small cell lung cancer: visualization by positron emission tomography in a patient harboring a mutation in the epidermal growth factor receptor. *J Thorac Oncol.* (2011) 6:1287–9. doi: 10.1097/JTO.0b013e318219ab87

178. Petrulli JR, Sullivan JM, Zheng MQ, Bennett DC, Charest J, Huang Y, et al. Quantitative analysis of [11C]-erlotinib PET demonstrates specific binding for activating mutations of the EGFR kinase domain. *Neoplasia.* (2013) 15:1347–53. doi: 10.1593/neo.131666

179. Bahce I, Smit EF, Lubberink M, van der Veldt AA, Yaqub M, Windhorst AD, et al. Development of [(11)C]erlotinib positron emission tomography for in vivo evaluation of EGF receptor mutational status. *Clin Cancer Res.* (2013) 19:183–93. doi: 10.1158/1078-0432.Ccr-12-0289

180. Slobbe P, Windhorst AD, Stigter-van Walsum M, Smit EF, Niessen HG, Solca F, et al. A comparative PET imaging study with the reversible and irreversible EGFR tyrosine kinase inhibitors [(11)C]erlotinib and [(18)F]afatinib in lung cancer-bearing mice. *EJNMMI Res.* (2015) 5:14. doi: 10.1186/s13550-015-0088-0

181. Bahce I, Yaqub M, Smit EF, Lammertsma AA, van Dongen GA, Hendrikse NH. Personalizing NSCLC therapy by characterizing tumors using TKI-PET and immuno-PET. *Lung Cancer.* (2017) 107:1–13. doi: 10.1016/j.lungcan.2016.05.025

182. Yeh HH, Ogawa K, Balatoni J, Mukhapadhyay U, Pal A, Gonzalez-Lepera C, et al. Molecular imaging of active mutant L858R EGF receptor (EGFR) kinase-expressing nonsmall cell lung carcinomas using PET/CT. *Proc Natl Acad Sci USA.* (2011) 108:1603–8. doi: 10.1073/pnas.1010744108

183. Yeh SH, Lin CF, Kong FL, Wang HE, Hsieh YJ, Gelovani JG, et al. Molecular imaging of nonsmall cell lung carcinomas expressing active mutant EGFR kinase using PET with [(124)i]-morpholino-IPQA. *Biomed Res Int.* (2013) 2013:549359. doi: 10.1155/2013/549359

184. Sun X, Xiao Z, Chen G, Han Z, Liu Y, Zhang C, et al. A PET imaging approach for determining EGFR mutation status for improved lung cancer patient management. *Sci Transl Med.* (2018) 10:eaan8840. doi: 10.1126/scitranslmed.aan8840

185. Su H, Seimbille Y, Ferl GZ, Bodenstein C, Fueger B, Kim KJ, et al. Evaluation of [(18)F]gefitinib as a molecular imaging probe for the assessment of the epidermal growth factor receptor status in malignant tumors. *Eur J Nucl Med Mol Imaging.* (2008) 35:1089–99. doi: 10.1007/s00259-007-0636-6

186. Sierra JR, Tsao MS. c-MET as a potential therapeutic target and biomarker in cancer. *Ther Adv Med Oncol.* (2011) 3(Suppl 1):S21–35. doi: 10.1177/1758834011422557

187. Ou SH. Crizotinib: a drug that crystallizes a unique molecular subset of non-small-cell lung cancer. *Expert Rev Anticancer Ther.* (2012) 12:151–62. doi: 10.1586/era.11.186

188. Krishnaswamy S, Kanteti R, Duke-Cohan JS, Loganathan S, Liu W, Ma PC, et al. Ethnic differences and functional analysis of MET mutations in lung cancer. *Clin Cancer Res.* (2009) 15:5714–23. doi: 10.1158/1078-0432.Ccr-09-0070

189. Du X, Shao Y, Qin HF, Tai YH, Gao HJ. ALK-rearrangement in non-small-cell lung cancer (NSCLC). *Thorac Cancer.* (2018) 9:423–30. doi: 10.1111/1759-7714.12613

190. Park S, Choi YL, Sung CO, An J, Seo J, Ahn MJ, et al. High MET copy number and MET overexpression: poor outcome in non-small cell lung cancer patients. *Histol Histopathol.* (2012) 27:197–207. doi: 10.14670/hh-27.197

191. Buck JR, Saleh S, Claus T, Lovly C, Hight MR, Nickels ML, et al. N-[(18)F]-Fluoroacetylcrizotinib: A potentially potent and selective PET tracer for molecular imaging of non-small cell lung cancer. *Bioorg Med Chem Lett.* (2020) 30:127257. doi: 10.1016/j.bmcl.2020.127257

192. Lin Q, Zhang Y, Fu Z, Hu B, Si Z, Zhao Y, et al. Synthesis and evaluation of (18)F labeled crizotinib derivative [(18)F]FPC as a novel PET probe for imaging c-MET-positive NSCLC tumor. *Bioorg Med Chem.* (2020) 28:115577. doi: 10.1016/j.bmc.2020.115577

193. Perera S, Piwnica-Worms D, Alauddin MM. Synthesis of a [(18)F]-labeled ceritinib analogue for positron emission tomography of anaplastic lymphoma kinase, a receptor tyrosine kinase, in lung cancer. *J Labelled Comp Radiopharm.* (2016) 59:103–8. doi: 10.1002/jlcr.3373

194. Lindner T, Loktev A, Giesel F, Kratochwil C, Altmann A, Haberkorn U. Targeting of activated fibroblasts for imaging and therapy. *EJNMMI Radiopharm Chem.* (2019) 4:16. doi: 10.1186/s41181-019-0069-0

195. Park JE, Lenter MC, Zimmermann RN, Garin-Chesa P, Old LJ, Rettig WJ. Fibroblast activation protein, a dual specificity serine protease expressed in reactive human tumor stromal fibroblasts. *J Biol Chem.* (1999) 274:36505–12. doi: 10.1074/jbc.274.51.36505

196. Henry LR, Lee HO, Lee JS, Klein-Szanto A, Watts P, Ross EA, et al. Clinical implications of fibroblast activation protein in patients with colon cancer. *Clin Cancer Res.* (2007) 13:1736–41. doi: 10.1158/1078-0432.Ccr-06-1746

197. Giesel FL, Heussel CP, Lindner T, Röhrich M, Rathke H, Kauczor HU, et al. FAPI-PET/CT improves staging in a lung cancer patient with cerebral metastasis. *Eur J Nucl Med Mol Imaging.* (2019) 46:1754–5. doi: 10.1007/s00259-019-04346-z

198. Loktev A, Lindner T, Burger EM, Altmann A, Giesel F, Kratochwil C, et al. Development of fibroblast activation protein-targeted radiotracers with improved tumor retention. *J Nucl Med.* (2019) 60:1421–9. doi: 10.2967/jnumed.118.224469

199. Koerber SA, Staudinger F, Kratochwil C, Adeberg S, Haefner MF, Ungerechts G, et al. The Role of (68)Ga-FAPI PET/CT for Patients with Malignancies of the Lower Gastrointestinal Tract: First Clinical Experience. *J Nucl Med.* (2020) 61:1331–6. doi: 10.2967/jnumed.119.237016

200. Giesel FL, Adeberg S, Syed M, Lindner T, Jiménez-Franco LD, Mavriopoulou E, et al. FAPI-74 PET/CT Using Either (18)F-AlF or Cold-Kit (68)Ga Labeling: Biodistribution, Radiation Dosimetry, and Tumor Delineation in Lung Cancer Patients. *J Nucl Med.* (2021) 62:201–7. doi: 10.2967/jnumed.120.245084

201. Loktev A, Lindner T, Mier W, Debus J, Altmann A, Jäger D, et al. A Tumor-Imaging Method Targeting Cancer-Associated Fibroblasts. *J Nucl Med.* (2018) 59:1423–9. doi: 10.2967/jnumed.118.210435

202. Gandini S, Massi D, Mandalà M. PD-L1 expression in cancer patients receiving anti PD-1/PD-L1 antibodies: A systematic review and meta-analysis. *Crit Rev Oncol Hematol.* (2016) 100:88–98. doi: 10.1016/j.critrevonc.2016.02.001

203. Natarajan A, Mayer AT, Xu L, Reeves RE, Gano J, Gambhir SS. Novel Radiotracer for immunopet imaging of PD-1 checkpoint expression on tumor infiltrating lymphocytes. *Bioconjug Chem.* (2015) 26:2062–9. doi: 10.1021/acs.bioconjchem.5b00318

204. Maute RL, Gordon SR, Mayer AT, McCracken MN, Natarajan A, Ring NG, et al. Engineering high-affinity PD-1 variants for optimized immunotherapy and immuno-PET imaging. *Proc Natl Acad Sci USA.* (2015) 112:E6506–14. doi: 10.1073/pnas.1519623112

205. Bao R, Wang Y, Lai J, Zhu H, Zhao Y, Li S, et al. Enhancing Anti-PD-1/PD-L1 Immune Checkpoint Inhibitory Cancer Therapy by CD276-Targeted Photodynamic Ablation of Tumor Cells and Tumor Vasculature. *Mol Pharmaceut.* (2019) 16:339–48. doi: 10.1021/acs.molpharmaceut.8b00997

206. Lv G, Sun X, Qiu L, Sun Y, Li K, Liu Q, et al. PET Imaging of Tumor PD-L1 Expression with a Highly Specific Nonblocking Single-Domain Antibody. *J Nucl Med.* (2020) 61:117–22. doi: 10.2967/jnumed.119.226712

207. Chatterjee S, Lesniak WG, Miller MS, Lisok A, Sikorska E, Wharram B, et al. Rapid PD-L1 detection in tumors with PET using a highly specific peptide. *Biochem Biophys Res Commun.* (2017) 483:258–63. doi: 10.1016/j.bbrc.2016.12.156

208. De Silva RA, Kumar D, Lisok A, Chatterjee S, Wharram B, Venkateswara Rao K, et al. Peptide-Based (68)Ga-PET Radiotracer for Imaging PD-L1 Expression in Cancer. *Mol Pharm.* (2018) 15:3946–52. doi: 10.1021/acs.molpharmaceut.8b00399

209. Lesniak WG, Mease RC, Chatterjee S, Kumar D, Lisok A, Wharram B, et al. Development of [(18)F]FPy-WL12 as a PD-L1 Specific PET Imaging Peptide. *Mol Imaging.* (2019) 18:1536012119852189. doi: 10.1177/1536012119852189

210. Zhou X, Jiang J, Yang X, Liu T, Ding J, Nimmagadda S, et al. First-in-human evaluation of a PD-L1-binding peptide radiotracer in non-small cell lung cancer patients with PET. *J Nucl Med Jnumed.* (2021) 121:262045. doi: 10.2967/jnumed.121.262045

211. Foss CA, Mease RC, Cho SY, Kim HJ, Pomper MG. GCPII imaging and cancer. *Curr Med Chem.* (2012) 19:1346–59. doi: 10.2174/092986712799462612

212. Damjanovic J, Janssen JC, Furth C, Diederichs G, Walter T, Amthauer H, et al. (68) Ga-PSMA-PET/CT for the evaluation of pulmonary metastases and opacities in patients with prostate cancer. *Cancer Imaging.* (2018) 18:20. doi: 10.1186/s40644-018-0154-8

213. Liu H, Rajasekaran AK, Moy P, Xia Y, Kim S, Navarro V, et al. Constitutive and antibody-induced internalization of prostate-specific membrane antigen. *Cancer Res.* (1998) 58:4055–60.

214. Afshar-Oromieh A, Haberkorn U, Eder M, Eisenhut M, Zechmann CM. [68Ga]Gallium-labelled PSMA ligand as superior PET tracer for the diagnosis of prostate cancer: comparison with 18F-FECH. *Eur J Nucl Med Mol Imaging.* (2012) 39:1085–6. doi: 10.1007/s00259-012-2069-0

215. Rowe SP, Drzezga A, Neumaier B, Dietlein M, Gorin MA, Zalutsky MR, et al. Prostate-Specific Membrane Antigen-Targeted Radiohalogenated PET and Therapeutic Agents for Prostate Cancer. *J Nucl Med.* (2016) 57(Suppl 3):90s–6s. doi: 10.2967/jnumed.115.170175

216. Afshar-Oromieh A, Malcher A, Eder M, Eisenhut M, Linhart HG, Hadaschik BA, et al. PET imaging with a [68Ga]gallium-labelled PSMA ligand for the diagnosis of prostate cancer: biodistribution in humans and first evaluation of tumour lesions. *Eur J Nucl Med Mol Imaging.* (2013) 40:486–95. doi: 10.1007/s00259-012-2298-2

217. Schmidt LH, Heitkötter B, Schulze AB, Schliemann C, Steinestel K, Trautmann M, et al. Prostate specific membrane antigen (PSMA) expression in non-small cell lung cancer. *PLoS One.* (2017) 12:e0186280. doi: 10.1371/journal.pone.0186280

218. Jochumsen MR, Gormsen LC, Nielsen GL. 68Ga-PSMA Avid Primary Adenocarcinoma of the Lung With Complementary Low 18F-FDG Uptake. *Clin Nucl Med.* (2018) 43:117–9. doi: 10.1097/rlu.0000000000001935

219. Pyka T, Weirich G, Einspieler I, Maurer T, Theisen J, Hatzichristodoulou G, et al. 68Ga-PSMA-HBED-CC PET for differential diagnosis of suggestive lung lesions in patients with prostate cancer. *J Nucl Med.* (2016) 57:367–71. doi: 10.2967/jnumed.115.164442

220. Virgolini I, Decristoforo C, Haug A, Fanti S, Uprimny C. Current status of theranostics in prostate cancer. *Eur J Nucl Med Mol Imaging.* (2018) 45:471–95. doi: 10.1007/s00259-017-3882-2

221. Shetty D, Loh H, Bui C, Mansberg R, Stevanovic A. Elevated 68Ga prostate-specific membrane antigen activity in metastatic non-small cell lung cancer. *Clin Nucl Med.* (2016) 41:414–6. doi: 10.1097/rlu.0000000000001139

222. NCCN,. *NCCN Guidelines*. (2021). Available online at: https://www.nccn.org/guidelines/category_1 (accessed April 15, 2022).